NanoImpact 14 (2019) 100158

Contents lists available at ScienceDirect

NanoImpact

journal homepage: www.elsevier.com/locate/nanoimpact

Research paper

Ranking of nanomaterial potency to induce pathway perturbations associated with lung responses

Sabina Halappanavar[a,*], Luna Rahman[a], Jake Nikota[a], Sarah S. Poulsen[b], Yaobo Ding[d,e], Petra Jackson[b], Hakan Wallin[c], Otmar Schmid[d,e], Ulla Vogel[b], Andrew Williams[a]

[a] Environmental Health Science and Research Bureau, Health Canada, Ottawa, Ontario, Canada
[b] The National Research Centre for the Working Environment, Copenhagen, Denmark
[c] STAMI, National Institute of Occupational Health, Gydas vei 8, 0363 Oslo, Norway
[d] Comprehensive Pneumology Center Munich (CPC-M), Member of the German Center for Lung Research (DZL), Munich 81377, Germany
[e] Institute of Lung Biology and Disease, Helmholtz Zentrum München - German Research Center for Environmental Health, Neuherberg, Munich 85764, Germany

ARTICLE INFO

Keywords:
Bench Mark Dose modelling
Transcriptional Bench Mark Dose
Bench Mark Dose for neutrophil infiltration
Carbon nanotubes
Nano titanium dioxide
Carbon black

ABSTRACT

Global transcriptomic responses in lungs of mice exposed for 24 h to individual multi-walled carbon nanotubes (MWCNTs, ten different types), nano titanium dioxide (nano TiO_2, nine different types) and one type of carbon black (CB) nanomaterials (NMs) were investigated using toxicogenomics tools to determine if gene or pathway dose-response modelling can be used to rank the potential of NMs to induce *in vivo* acute lung inflammation.

In each study, female adult C57BL/6 mouse lungs were intratracheally exposed once with 18, 54 or 162 μg/mouse doses of individual NMs and control mice were exposed to vehicle only. A high dose of 486 μg/mouse was used in only one study that involved nanoTiO_2. The pathway perturbations associated with NM features and the underlying toxicity mechanisms were identified using bioinformatics tools. Bench Mark Dose (BMD) response analysis was conducted to derive transcriptional BMD estimates for each differentially expressed gene and the associated pathways in NM-treated lungs compared to vehicle-treated controls. The resulting BMDs were used to rank the potency of different NMs to induce perturbations in pathways that mark the occurrence of acute lung inflammation in mice. The transcriptional BMDs were compared with the BMDs of an apical endpoint derived for the lung neutrophil influx in bronchoalveolar lavage fluid from the same mice, a commonly measured pro-inflammatory endpoint *in vivo*.

The results showed that similar gene and pathway responses were induced by the NM variants investigated. Among the MWCNT types, NM-401 and Mitsui-7, the two long and rigid fibres exhibited the most potency and, the short and tangled NRCWE-026 exhibited the least potency compared to the other nine varieties. Although mixed rutile/anatase nano TiO_2 showed higher potency compared to other nano TiO_2, owing to the large confidence intervals, a clear distinction in potency could not be made. CB behaved similarly to the less potent MWCNTs. The transcriptomic BMDs were largely comparable to the neutrophil influx BMDs, with mass-based BMDs showing better correlation for all approaches. The mass-based BMDs were more conservative compared to the surface area based BMDs. Although the NMs investigated did not show large differences in their responses that would allow a clear ranking, the concept described demonstrates that quantitative pathway responses can be used to rank the potency of NMs to induce *in vivo* lung inflammation.

1. Introduction

Nanomaterials (NMs), materials having at least one dimension of their structure in a size range of 1–100 nm, are synthesised in a massive scale and are widely used in many consumer products. NMs are different from their chemically identical bulk counterparts; they come in

Abbreviations: MWCNT, multi-walled carbon nanotubes; CB, carbon black; NM, nanomaterial; nano TiO_2, nano titanium dioxide; BMD, Bench Mark Dose; BMDt, Transcriptional Bench Mark Dose; BMDneu, Bench Mark Dose for neutrophil infiltration; BMD-M, Bench Mark Dose based on mass; BMD-SA, Bench Mark Dose based on surface area; BALF, Bronchoalveolar lavage fluid; IPA, Ingenuity Pathway Analysis; AIC, Akaike Information Criterion; DEG, differentially expressed genes; AOP, adverse outcome pathway

* Corresponding author.
E-mail address: Sabina.halappanavar@canada.ca (S. Halappanavar).

https://doi.org/10.1016/j.impact.2019.100158
Received 21 December 2018; Received in revised form 8 April 2019; Accepted 9 April 2019
Available online 29 April 2019

various shapes and forms, the physico-chemical properties of which vary depending on their intended applications. Several of these physico-chemical properties (*e.g.*, shape, surface area, chemical composition, solubility and charge) have been shown to significantly influence their ability to induce toxicity (Maynard et al., 2010; Geraci and Castranova, 2010; Johnston et al., 2013; Noel et al., 2012; Warheit et al., 2007). To date, using the available toxicity data, it has not been possible to derive a property-toxicity response matrix for any individual NM, or rank and group NMs according to their toxic potency.

From the existing *in vivo* and *in vitro* studies reporting on the biological behaviour and cellular effects of NMs, it can be consistently concluded that they are easily aerosolised and, inhalation is the most common and extensively investigated route of exposure to NMs (Borm et al., 2006). A significant fraction of respirable NMs can reach the distal alveolar region of the lung, which is more vulnerable than the mucus-protected bronchial region, relying mainly on phagocytic clearance by the alveolar macrophages as protection mechanism (Kreyling et al., 2009). In general, the alveolar NM dose increases with exposure levels and persists for an extended period of time even after NM exposure has ceased causing long-term damage to the lung cells (Kreyling and Scheuch, 2000). The particle size is a critical parameter not only in determining how deep the particles travel into the lung and into the tissue, it is also associated to its mass-specific surface area, which is one of the most relevant determinants of their acute and chronic toxicity (Schmid and Stoeger, 2016; Maynard and Kuempel, 2005). Most NMs, when inhaled, induce dose-dependent increase in the levels of pro-inflammatory mediators (cytokines, chemokines, growth factors), acute phase response proteins, and influx of pro-inflammatory cells in the lung lining fluid (bronchoalveolar lavage fluid, BALF) resulting in lung inflammation (Saber et al., 2013), a widely observed tissue response. Lung fibrosis is the commonly noted pathology for NMs in mice, and genotoxicity (Sargent et al., 2012), carcinogenicity (Kasai et al., 2015; Sargent et al., 2014; Yann et al., 2014) and mesothelioma (Takagi et al., 2012) are the less frequently observed adverse outcomes. The pathogenic potential of NMs is generally attributed to their shape, surface area to mass ratio (Schmid and Stoeger, 2016; Maynard and Kuempel, 2005), level and duration of exposure and tissue persistence (Pietroiusti et al., 2018). The other routes of exposure to NMs including the gastrointestinal or dermal route are less characterised in comparison to inhalation. While existing evidence suggests that intact lung tissue is an effective albeit not a perfect barrier against NM penetration following inhalation exposure (Kreyling et al., 2013), gastrointestinal exposure is suggested to play an important role in human exposure to NMs as the NM application in food and consumer products is expected to escalate in the future (Pietroiusti et al., 2018). In addition to the above, a limited number of underlying mechanisms of response have been identified for NMs, which include the potential to induce reactive oxygen species (ROS) synthesis, genotoxicity and pro-inflammatory responses. However, due to the various issues associated with NM toxicity testing, the available toxicity data is deemed not suitable or insufficient to support regulatory decision making or conduct human health risk assessment of NMs.

The issues related to testing NMs are many, which include their sheer number and versatile properties. In addition, significant deficiencies in the data such as insufficient physico-chemical characterisation of NMs, use of human irrelevant doses, inconsistent testing and reporting standards, and lack of *in vivo* relevance of *in vitro* data have impeded the applicability of the existing data in quantitative assessments of risks posed by NMs and meaningful comparisons of biological responses/effects induced by the diverse NMs (Kuempel et al., 2012; Warheit, 2018). This, in turn, has made it difficult to apply conventional read-across or grouping strategies to categorise NMs in their respective toxicity groups.

Thus, timely toxicological assessment of every individual NM using the conventional toxicity testing tools and strategies is not a feasible option. Alternatively, sensitive high content molecular-level tools that can comprehensively and effectively discern the diverse property-specific responses, identifying the underlying toxicity mechanisms are needed. Genome-wide analysis of expression patterns, *e.g.* transcriptomics analysis to examine genes and associated biological pathways that are perturbed following exposure has proven useful in revealing the underlying mechanisms of substance-induced toxicity including NMs. For the chemical substances, it has been shown that structurally similar chemicals or compounds belonging to a common class induce similar patterns of gene expression, elicit similar toxicity and thus, transcriptomics can be used to identify chemical categories or classify chemicals (Hamadeh et al., 2002). The transcriptomics data are used to connect chemicals, genes and diseases (Lamb et al., 2006), to support identification of key events involved in the pathogenesis (Bercu et al., 2010; Labib et al., 2016a; Chepelev et al., 2016), to establish new (Labib et al., 2016b) and apply already described adverse outcome pathways (AOPs) (Brockmeier et al., 2017), to discover novel biomarkers of effect, to predict toxicity (Kohonen et al., 2017), and to support substance prioritisation, categorisation and read-across (Sauer et al., 2017; Buesen et al., 2017). In recent years, multiple studies have used the benchmark dose (BMD) method to evaluate the dose-response changes in individual genes or pathways (Thomas et al., 2007; Thomas et al., 2010; Thomas et al., 2012). BMD is the dose or concentration of a toxicant that induces a predetermined level of response (Bench Mark Response) above or below the response observed in the control samples. BMD modelling is the preferred approach for deriving point of departure (POD) for developing reference dose or safe dose estimates or other risk values such as acceptable daily intake values. The statistical lower confidence bound on the BMD (BMDL), which is a conservative estimate of the dose at which a specific response is observed, is used by the regulatory agencies to set safe exposure levels. BMD modelling takes into account the entire dose-response curve and allows cross comparison of the studies *via* use of consistent response levels (benchmark response) across studies or study types. On the contrary, the use of the no-observed adverse-effect level (NOAEL) is limited to the doses tested in an experiment, making it difficult to compare the responses across studies as the observed response at a specific NOAEL may vary between the studies. The BMD approach also considers the size of the study and allows estimation of the probability of a response at any dose level, which is not true for the NOAEL approach (Haber et al., 2018). The dose identified by the BMD analysis should be related to the tissue-delivered dose, which can then be translated into equivalent human concentrations (Schmid and Cassee, 2017). BMD analysis enables incorporation of dose-response information and helps identify doses at which the pathway responses to NM exposure were significantly perturbed compared to the relative controls. These studies have shown concordance between the transcriptional/pathway BMDs and the conventional apical cancer and non-cancer endpoint BMDs, suggesting that the transcriptional responses can potentially be used to estimate points of departures (PODs) for chemical-induced toxicity in support of both cancer and non-cancer risk assessment (Moffat et al., 2015).

In the context of numerous NMs of wide diversity, the transcriptomics data can be effective: 1) in supporting toxicity screening or ranking strategies, enabling binning of NMs into low, moderate or high toxicity categories or decision support systems for categorising NMs into different risk classes, 2) in reasonable prioritisation of NMs that may require immediate and detailed toxicological assessments, and 3) to rank the potency of NMs to induce specific toxicity. It is envisioned that global understanding of the biology perturbed and a detailed profiling of the molecular signatures altered following exposure to NMs will enable effective characterisation of the toxicity mechanisms at play and help define the properties that predict adverse outcomes.

In the present study, global gene expression profiles derived from mice following lung exposure to different types of NMs of diverse properties were compiled. The NMs included were multi- walled carbon nanotubes (MWCNTs) including Mitsui-7/MWCNT-7 (Grosse et al., 2014), carbon black (CB) (IARC monographs on the evaluation of

carcinogenic risks to humans: carbon black, titanium dioxide, and talc, 2010) and TiO_2 nanoparticles (nano TiO_2), all of which are classified as possibly carcinogenic to humans (IARC monographs on the evaluation of carcinogenic risks to humans: carbon black, titanium dioxide, and talc, 2010). The main objective of the study was to explore if transcriptomics or pathway dose-response modelling can be used to rank the potential of NMs to induce perturbations in pathways indicative of acute lung responses commonly induced by inhaled NMs. In brief, unpublished and published in-house microarray transcriptomics data from mouse lungs 24 h after intratracheal deposition of individual NM types, including MWCNTs, CB, and nano TiO_2 of varying properties were used to derive the gene and pathway BMD estimates. To represent the widely varying physico-chemical properties of nano TiO_2 and MWCNTs (Jackson et al., 2015a; Halappanavar et al., 2015) a panel of 10 different MWCNTs, 9 variants of nano TiO_2 and one CB type were included. Specifically, we included the MWCNT Mitsui-7, the nano TiO_2 NM-105 (also called P25) and the CB (Printex90), all of which have been shown to cause lung cancer by inhalation in rats (Kasai et al., 2016; Heinrich et al., 1995). Bioinformatics tools were applied to identify the pathway perturbations associated with NM features and to identify the underlying mechanisms of toxicity. BMD response analysis, both in terms of mass (BMD-M) and surface area (BMD-SA) as dose metric was conducted to derive dose-response values for each gene that was differentially expressed and the associated pathways in NM-treated lungs compared to vehicle-treated matched controls. The resulting transcriptional BMDs were used to rank the potency of different NMs to induce perturbations in pathways that mark the occurrence of lung inflammation in mice. The transcriptional BMDs were compared with the BMDs of an apical endpoint derived for the neutrophil influx in BALF from the same mice (24 h after NM instillation), a commonly measured pro-inflammatory endpoint *in vivo*.

2. Methods

2.1. Materials and studies included in the analysis

The individual NMs included in the analysis differed in their chemical composition and physico-chemical properties, and were characterised for primary size, surface area according to the Brunauer-Emmet-Teller method (BET), semi-quantitative elemental analysis, in addition to other material specific properties. Table 1 summarises the studies that were included in the dose-response analysis, consisting of experimental details such as the type of NM, mode of exposure, strain of mouse, dose, post-exposure time point investigated and the microarray platform used (Poulsen et al., 2013). Table 2 lists the NM ID, vendor's name and primary physico-chemical characteristics of NMs. Only in-house studies that investigated the gene expression profiles in lungs following NM exposure were included. All microarray data are available through the Gene Expression Omnibus (GEO) (http://www.ncbi.nlm.nih.gov/geo).

Details of the study design, animal exposures, necropsy and methodology for various endpoints including microarray experiments have been reported previously (Poulsen et al., 2013; Poulsen et al., 2015; Bourdon et al., 2012; Halappanavar et al., 2015; Husain et al., 2013). Animal exposures conducted at the National Research Centre for the Working Environment (Denmark) complied with the EC Directive 86/609/EEC and Danish law regulating experiments with animals (The Danish Ministry of Justice, Animal Experiments Inspectorate, permission 2006/561-1123) and the exposures conducted at Health Canada (Canada) complied with the guidelines of the Canadian Council for Animal Care and approved by Health Canada's Animal Care Committee. All studies involved had similar experimental designs, which included single intratracheal instillation of female adult C57BL/6 mouse lungs with 6, 18, 54 and 162 µg/mouse doses of individual NMs. NMs were dispersed in MilliQ water containing 2% serum (MWCNTs), in MilliQ water containing 0.9% NaCl and 10% v/v acellular BALF (nano TiO_2,

Table 1
Details of the published and unpublished studies included in the analysis.

Reference	Nanomaterial/chemical	Route of exposure	Mouse strain	Dose (µg/mouse)	Post-exposure time point	Array platform	GSE
Halappanavar et al. (in press, NANOIMPACT)	Multi-walled carbon nanotubes	Intratracheal instillation	Adult C57BL/6	Single instillation. 18, 54	24 h	Agilent whole genome	GSE124041
Poulsen et al. (2013)	Multi-walled carbon nanotubes	Intratracheal instillation	Adult C57BL/6	Single instillation. 18, 54, 162	24 h	Agilent whole genome	GSE47000
Poulsen et al. (2015)	Multi-walled carbon nanotubes	Intratracheal instillation	Adult C57BL/6	Single instillation. 18, 54, 162	24 h	Agilent whole genome	GSE35284
Bourdon et al. (2012)	Carbon black	Intratracheal instillation	Adult C57BL/6	Single instillation. 18, 54, 162	24 h	Agilent whole genome	GSE35193
Halappanavar et al. (2015)	Nano titanium dioxide	Intratracheal instillation	Adult C57BL/6	Single instillation. 18, 54, 162	24 h	Agilent whole genome	GSE60801
Rahman et al. (2016)	Nano titanium dioxide	Intratracheal instillation	Adult C57BL/6	Single instillation. 18, 54, 162 or 486	24 h	Agilent whole genome	GSE65623

Table 2
Details of the NM characteristics.

Reference	Name of NM as published	Producer (particle name)	BET (m^2/g)	Size (nm)	Length (nm ± SD)	Diameter (nm ± SD)
Halappanavar et al. (unpublished)	NRCWE-043	Cheap Tubes, Brattleboro, VT	82		771.3(± 3471)	26.73(± 6.88)
	NRCWE-044	Cheap Tubes, Brattleboro, VT	74		1330(± 2454)	32.55(± 14.44)
	NRCWE-045	Cheap Tubes, Brattleboro, VT	119		1553(± 2954)	28.07(± 13.85)
	NRCWE-046	Cheap Tubes, Brattleboro, VT	223		717.2(± 1214)	17.22(± 5.77)
	NRCWE-047	Cheap Tubes, Brattleboro, VT	216		532.5(± 591.9)	12.96(± 4.44)
	NRCWE-048	Cheap Tubes, Brattleboro, VT	185		1604(± 5609)	15.08(± 4.69)
	NRCWE-049	Cheap Tubes, Brattleboro, VT	199		731.1(± 1473)	13.85(± 6.09)
Poulsen et al. (2013)	Mitsui-7	Mitsui/Hadoga	26		5.700(± 0.490)	74(29–173)
Poulsen et al. (2015)	CNT_{small} (NRCWE-026)	Nanocyl (NC-7000)	245.8		850(± 457)	11(± 4.5)
Jackson et al. (2015a, 2015b)	CNT_{large} (NM-401)	OECD WPMN	14.6–18		4000(± 2400)	67(± 2.40)
Jackson et al. (2015a, 2015b)	CBNPs	Evonik/Degussa (Printex 90)	182	14		
Halappanavar et al. (2015)	$TiO_2NP^{10.5}$ (NRCWE-030)	NanoAmor	139.1	10.5		
	TiO_2NP^{38} (NRCWE-025)	Nabond	28.2	38		
	TiO_2NP^{10} (NRCWE-001)	NanoAmor	99	10		
	TiO_2NP^{10+} (NRCWE-002)	NanoAmor	84	10		
Rahman et al. (2016)	$^{a}TiO_2^{8}$	OECD - WPMN, available through Sachtleben Chemie GmbH, Germany (Hombikat UV100)	234.47–229.0	8		
	$^{a}TiO_2^{20}$	OECD - WPMN, Cristal Global (PC105)	90	20		
	$^{ra}TiO_2^{20}$	OECD - WPMN, Evonik Degussa GmbH, Germany (P25)	52.81–55.49	22		
	$^{r}TiO_2^{20}$ (HY)	OECD - WPMN, available through Sachtleben Chemie GmbH, Germany (UV Titan M262)	51.69–50.86	20		
	$^{r}TiO_2^{20}$ (HP)	OECD - WPMN, available through Sachtleben Chemie GmbH, Germany (UV Titan M212)	57.07–57.18	21		
	$^{a}TiO_2^{300}$	OECD - WPMN, Cristal Global (Tiona)	10	300		

CB) or in MilliQ water (nano TiO_2). Control mice were exposed to respective vehicle only. A high dose of 486 μg/mouse was used in only one study that involved nano TiO_2 (Rahman et al., 2016). The experimental design and methodological details for the data used from an unpublished study involving MWCNTs (NRCWE-043 – NRCWE-049) were the same as indicated above for the previously published studies except that the doses were 6, 18 and 54 μg/mouse, of which transcriptomic analyses was conducted for 18 and 54 μg/mouse dose groups. Thus, for MWCNTs NRCWE-043 - NRCWE-049, BMD analysis was conducted using only two doses. The results are summarised in Supplementary File −1.

2.1.1. Statistical and BMD analysis of microarray data

2.1.1.1. Statistical normalization of microarray data. The Agilent Whole Genome microarray platform was consistently used in all studies included in the analysis. Each microarray data set was individually analysed and a common statistical normalization method was applied. In brief, normalization and analysis of the data were conducted in the R environment as described in Nikota et al. (2015) (Nikota et al., 2015). The negative control 3xSLv1 probes were used to calculate the background fluorescence. A probe was considered absent if (within the background signal) the median signal intensities were less than the trimmed mean (trim = 5%) plus three trimmed standard deviations. A probe was considered present if at least four out of the five samples within an experimental condition showed signal intensities greater than the background measurements (defined above). Data were normalized using Locally WEighted Scatterplot Smoothing (LOWESS) (Labib et al., 2013; Yang et al., 2002), and ratio intensity plots and heat maps of the raw and normalized data were used to identify outliers. Differentially expressed genes (DEGs)—increasing or decreasing relative to the age matched control mice—were determined using the MicroArray ANalysis Of VAriance (MAANOVA) library in R (Wu et al., 2003; Parmigiani et al., 2003). This statistical model included the fixed effects of slide and treatment condition, and was applied to the $\log_2$ of the relative intensities. The Fs statistic was used to test for treatment effects (Cui et al., 2005). The permutation method that consisted of residual shuffling was used to calculate the p values for all statistical tests and the false discovery rate (FDR) approach was applied to adjust for multiple comparisons (Benjamini and Hochberg, 1995). A gene was considered significant if the FDR adjusted p value of the fold change in the experimental group relative to the control was < 0.05.

2.1.2. Preliminary analysis of the gene expression data

Subsequent to normalization of the gene expression data, a short-list of DEGs was generated using the criteria of an absolute fold change ≥ 1.5 and an FDR p-value < 0.05. Ingenuity Pathway Analysis knowledgebase (IPA, Ingenuity Systems, Redwood City, CA, USA) was used to identify the perturbed pathways and functions. The results were published previously. For the NRCWE-043 - 049, the results of the IPA analysis are summarised in the Supplementary File 1.

2.2. Benchmark dose modelling of transcriptional data

Only the 24 h time point was included in the analysis since a large number of genes showed altered expression at this early post-exposure time point. For the pathway BMD response modelling, the normalized gene expression data from mouse lungs exposed to a variety of NMs (Table 2) were used. Since some datasets used in the analysis consisted of only two doses, readily available and routinely used BMDExpress modelling software could not be applied, which requires a minimum of three doses. As a result, separate codes were written to calculate pathway BMDs in this study. In brief, the R statistical language (Team, R. C., 2014) and the bmd and drc (Ritz and Streibig, 2005) R libraries were used. Briefly, R code was written to calculate the median pathway BMD for which Ingenuity Pathway Analysis knowledgebase (IPA, Ingenuity Systems, Redwood City, CA, USA) gene sets were altered based on lung microarray data. First, MAANOVA (Wu et al., 2003; Cui et al., 2005) was conducted and the probe list was filtered using the FDR adjusted (Benjamini and Hochberg, 1995) Fs statistic (Cui et al., 2005) permutation based p-values with residual shuffling at the 0.05

significance level with a 1.5 fold change cut-off. The filtered $\log_2$ gene expression data was then centered using the mean of the control samples and the three, four and five parameter logistic and the two and three parameter log-logistic models were fit to the data using the bmd function with bench mark response level of 10% utilizing the relative risk definition of the BMD. The Akaike Information Criterion (AIC) was used for model selection, and the model with the lowest AIC value was used to select between the various models. Probes for which BMD values could be obtained were then mapped to IPA knowledgebase (IPA, Ingenuity Systems, Redwood City, CA, USA). Gene set enrichment analysis was then calculated for those IPA pathways with at least five probes/genes with BM estimates. Probes that showed BMD value higher than the highest dose were removed. The Fisher's Exact test was used to identify statistically significant gene sets with FDR adjusted p-value less than the 0.05 significance level. The median BMD was used to represent the gene set or pathway BMD. The bootstrap was used to estimate the lower bound for the pathway BMD. Other than the statistical cut-offs applied, in the present study, DEGs were not filtered to distinguish between biological and adverse changes. All DEGs (relative to untreated or vehicle treated controls) were considered for BMD estimation and gene set enrichment analysis was conducted for any pathway with a minimum of 5 DEGs and the BMD estimates for all significant pathways were reported. The obtained mass-based BMD values (BMD-M) were subsequently converted to the corresponding surface area-based BMDs (BMD-SA) by multiplying the BMD-M with the specific BET surface area for each NM. All BMD values are expressed in mass (BMD-M) unless otherwise stated (BMD-SA).

2.2.1. Estimating distributions for each approach

Distributions for the median BMD for the three approaches presented were estimated using the bootstrap (Effort and Tibshirani, 1993) as described in Farmahin et al. (2017). BMD estimates within pathways were randomly selected with replacement and the bootstrap median was estimated. A total of 2000 bootstraps were used to approximate the pathway BMD distribution for each of the three approaches.

2.3. Benchmark dose modelling of in vivo lung neutrophil influx

BMD analyses were carried out for BALF neutrophil counts using the freely available PROAST software (Version 61.2 – http://www.proast.nl). The data for all doses were fed as continuous data as the counts are large. The best fitting exponential model was selected based on the likelihood ratio test with more complex models with additional parameters only accepted if the difference in log-likelihood exceeds $p < 0.05$ and the Grubb criterion was used to remove any outliers. The benchmark response (BMR) used in the analysis was 10% representing a 10% increase in response relative to control. BMD values for neutrophil influx were expressed using both mass (BMD-M) and surface area (BMD-SA) as dose metric. R values represent the Pearson product-moment correlation estimates.

3. Results

3.1. Benchmark dose analysis of transcriptomic alterations

A statistical test was used to analyse the dose-response behaviour of genes and gene probe sets that showed significantly altered expression at the 24 hr post-exposure time point in treated compared to vehicle-only control samples. The number of probe sets showing significant dose-response behaviour at this post-exposure time point varied widely across the different NM types. The data that showed the best fit model were used as input for the IPA pathway analysis. A pathway BMD was calculated for any IPA pathway that consisted of a minimum of five DEGs from the lung transcriptomics data. BMD values for all IPA pathways that showed dose-response in each NM group are summarised in Supplementary Table 1 and are briefly described below by the NM group.

3.1.1. Canonical pathways perturbed following MWCNT exposure and the associated transcriptional BMD values

For the MWCNT group, 124, 96, 120, 83, 51, 25, 23, 175, 53, and 99 canonical pathways were significantly altered following exposure to Mitsui-7, NM-401, NRCWE-026, NRCWE-043, NRCWE-044, NRCWE-045, NRCWE-046, NRCWE-047, NRCWE-048 and NRCWE-049, respectively, for which calculated BMD-M values are presented in Supplementary Table 1. Of these, Agranulocyte Adhesion and Diapedesis (BMD/BMDL-M range - 3.56/0.73–112.44/9.80 μg/mouse), and Granulocyte Adhesion and Diapedesis (BMD/BMDL-M range - 22.88/8.69–97.33/3.81 μg/mouse) pathways associated with infiltration of inflammatory cells were consistently present across the panel of the 10 MWCNT groups (Supplementary Table 2). Acute Phase Response Signaling, Hepatic Fibrosis/Hepatic Stellate Cell Activation and Atherosclerosis Signaling were the other most commonly represented pathways. From the list of 20 most significant pathways from each of the individual MWCNT groups (Supplementary Table 2), pathways ($^{<}$FDR 0.05) that were present in at least three of the 10 individual MWCNT exposure groups and their BMD/BMDL-M distributions are shown in Fig. 1.

In general, BMD/BMDL-M values were close for the 20 pathways, except for NM-401, Mitsui-7, NRCWE-026 and NRCWE-044. BMD-M values for NRCWE-026 were large and scattered from below 20 μg/mouse to $^{>}$100 μg/mouse.

3.1.2. Enriched canonical pathways following nano TiO_2 exposure and the associated transcriptional BMD values

For the nano TiO_2 group, 22, 4, 78, 2, 18, 17, 16, 3, and 23 canonical pathways were significantly altered following exposure to $aTiO_2^{8}$, $aTiO_2^{20}$, $raTiO_2^{20}$, $rTiO_2^{20}$ (HP), $rTiO_2^{20}$ (HY), $aTiO2^{300}$, NRCWE-001, NRCWE-002, and NRCWE-030, respectively. There were no pathways in the NRCWE-025 group, for which BMDs could be derived. There were no pathways common across the panel of 9 nano TiO_2 and some of them presented with < 5 canonical pathways with BMD values. The three most prominent pathways were Acute Phase Response Signaling pathway (BMD/BMDL-M range -11.1/6.6–333.6/96.0 μg/mouse), which was significant in seven of the 9 different nano TiO_2 groups, as well as, Agranulocyte Adhesion and Diapedesis (BMD/BMDL-M range – 19.1/12.7–150.8/89.1 μg/mouse) and Granulocyte Adhesion and Diapedesis (BMD/BMDL-M range – 17.9/12.9–150.8/94.7 μg/mouse), which were perturbed in 6 of the 9 nano TiO_2 groups. Fig. 2 shows the BMD/BMDL-M distribution of the most significant pathways that were common to at least three of the nano TiO_2 exposure groups and the pathways are listed in Supplementary Table 2.

3.1.3. Canonical pathways perturbed following CB exposure and the associated transcriptional BMD values

There were 24 significant canonical pathways in the CB group, for which BMD estimates could be derived, and BMD/BMDL-M distribution for the 20 most significant (listed in Supplementary Table 2) of the 24 pathways is shown in Fig. 3. Similar to what was observed for the MWCNT and the nano TiO_2 groups, Agranulocyte Adhesion and Diapedesis (BMD/BMDL-M, 13.8/9.1 μg/mouse) and Granulocyte Adhesion and Diapedesis (BMD/BMDL-M, 13.0/7.5 μg/mouse) were altered following exposure to CB.

3.1.4. Pathway similarities between the NM groups

Ten (35.7%) canonical pathways from the list of 20 most significant pathways were common to all three NM groups. These included, Agranulocyte Adhesion and Diapedesis, Granulocyte Adhesion and Diapedesis, Acute Phase Response Signaling, LXR/RXR Activation, Atherosclerosis Signaling, IL-10 Signaling, Role of Macrophages, Fibroblasts and Endothelial Cells in Rheumatoid Arthritis, Role of IL-17F in Allergic Inflammatory Airway Diseases, IL-6 Signaling and

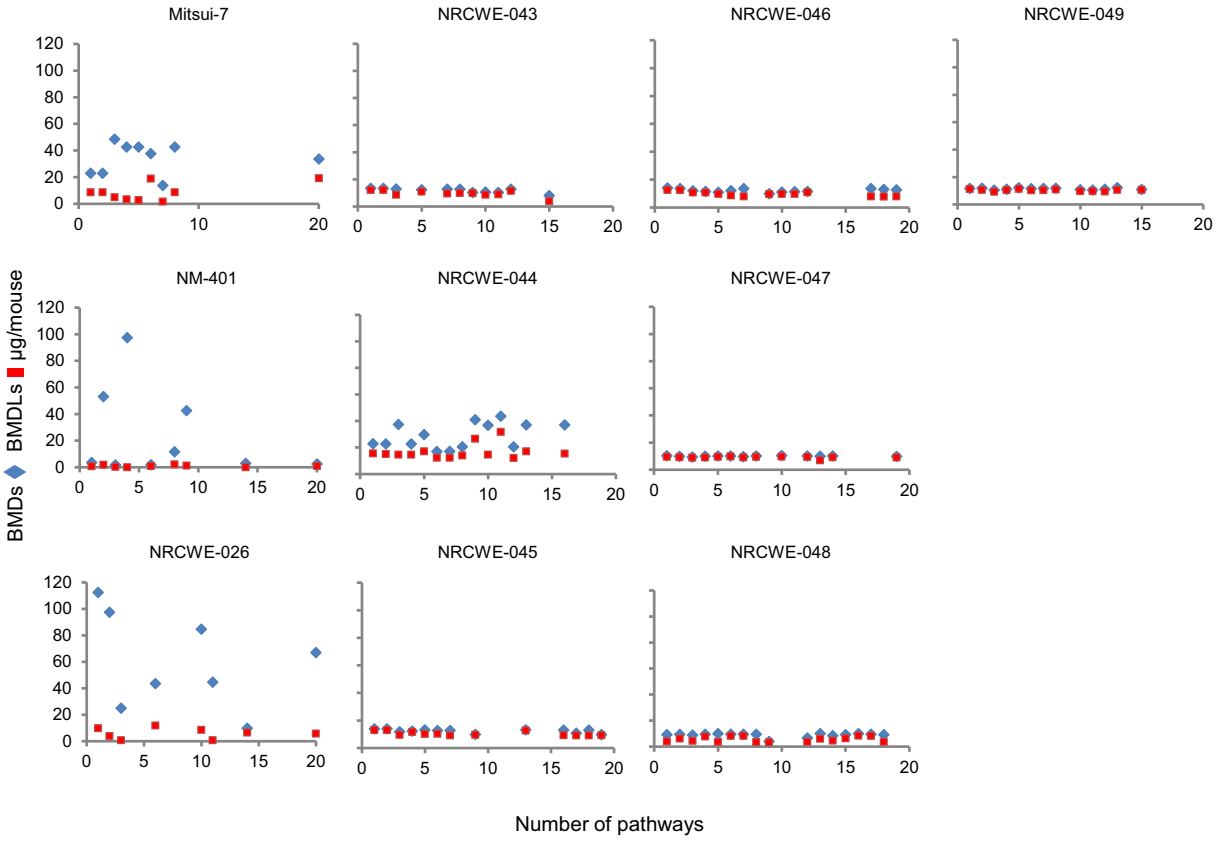

Fig. 1. Twenty most significant IPA pathways that were enriched in at least three of the MWCNT exposure groups and the associated BMD/BMDL (µg/mouse) values. Any pathway with FDR p value of < 0.05 was considered significant.

Hepatic Cholestasis pathways. The Cell Cycle Control of Chromosomal Replication, Xenobiotic Metabolism Signaling, Aryl Hydrocarbon Receptor Signaling, Leukocyte Extravasation Signaling, NF-κB Signaling, and Axonal Guidance Signaling pathways were unique to the MWCNT groups. Differential Regulation of Cytokine Production in Macrophages and T Helper Cells by IL-17A and IL-17F, IL-17A Signaling in Fibroblasts and Chemokine Signaling pathways were unique to CB. There were no pathways unique to nano TiO_2. It is important to note that the similarities and unique pathways described here are restricted to the pathways presented in Figs. 1–3.

3.1.5. Selection of pathways for consideration in potency estimation

Next, we applied three different approaches to select pathways and pathway BMDs for consideration in deriving POD estimates: 1) consideration of the pathway with the lowest transcriptional BMD estimate, 2) consideration of all perturbed pathways, for which transcriptional BMD could be estimated, 3) 10 pathways that were most significant and common to MWCNT, nano TiO_2 and CB groups (selected from Figs. 1–3). Results for each of these approaches were calculated in terms of mass, BMD-M (Figs. 4–6) and the respective specific surface area, BMD-SA (Figs. 7–9).

The results from approach 1 showed that the most sensitive pathway with the lowest BMD-M varied for each NM type (Fig. 4). Focussing first on MWCNTs, the pathways with the lowest transcriptional BMD estimates included, Triacylglycerol Biosynthesis (Mitsui-7), CD28 signaling in T helper cells (NM-401), Atherosclerosis Signaling (NRCWE-026), Angiopoietin Signaling (NRCWE-043), Corticotropin Releasing Hormone Signaling (NRCWE-044), RAR Activation (NRCWE-045), Mismatch Repair in Eukaryotes (NRCWE-046), Cell Cycle Control of Chromosomal Replication (NRCWE-047), Cell Cycle Control of Chromosomal Replication (NRCWE-048), and Role of CHK Proteins in Cell Cycle Checkpoint Control pathways (NRCWE-049). As expected, addition of more than one pathway with higher BMD values in the calculation of median pathway BMD-M (approach 2, Fig. 5 and approach 3, Fig. 6) increased the overall BMD-M estimates for all MWCNT types. Depending on the approach considered, differences were observed between the MWCNT types of different lengths or properties in their potency to induce pathway perturbations; for all approaches, NM-401 was the most potent of all MWCNT types, but the two least potent MWCNTs varied depending on the approach between Mitsui-7, NRCWE-026, and NRCWE-045. When using surface area as dose metric (BMD-SA) the MWCNT potency scaling became more coherent with NM-401 and Mitsui-7 showing the highest potency for all three approaches (Figs. 7–9) and NRCWE-026 representing the least potent MWCNTs for two out of the three approaches. However, the uncertainty in the BMD of NRCWE-026 was high for both mass and surface area as dose metric. Even with the large confidence intervals, NM-401 remained the most potent of all MWCNTs regardless of the approach or dose metric considered.

For the nano TiO_2 group, Role of Tissue Factor in Cancer ($aTiO_2^{8}$), Bladder Cancer Signaling ($aTiO_2^{20}$), LPS/IL-1 Mediated Inhibition of RXR Function ($raTiO_2^{20}$), Hepatic Fibrosis / Hepatic Stellate Cell Activation ($rTiO_2^{20}$ (HY)), Cell Cycle Control of Chromosomal Replication ($rTiO_2^{20}$ (HP)), IL-17 Signaling ($aTiO_2^{300}$), IL-6 signaling (NRCWE-001), Hepatic Fibrosis / Hepatic Stellate Cell Activation (NRCWE-002), and PI3K Signaling in B Lymphocytes (NRCWE-030) pathways showed the lowest BMD values. Although exhibiting large confidence intervals, by approach 1, the $raTiO_2^{20}$ and $rTiO_2^{20}$ (HP) ranked significantly high in potency compared to other nano TiO_2 types. The lowest transcriptional pathway BMD-M for $rTiO_2^{20}$ (HP) was much lower than that of $rTiO_2^{20}$ (HY) and $aTiO_2^{300}$. The observed differences in potency among TiO_2 types were mitigated with the inclusion of all pathways (approach 2, Fig. 5) or by including median BMD of 10 most significant pathways (approach 3, Fig. 6) mainly due to

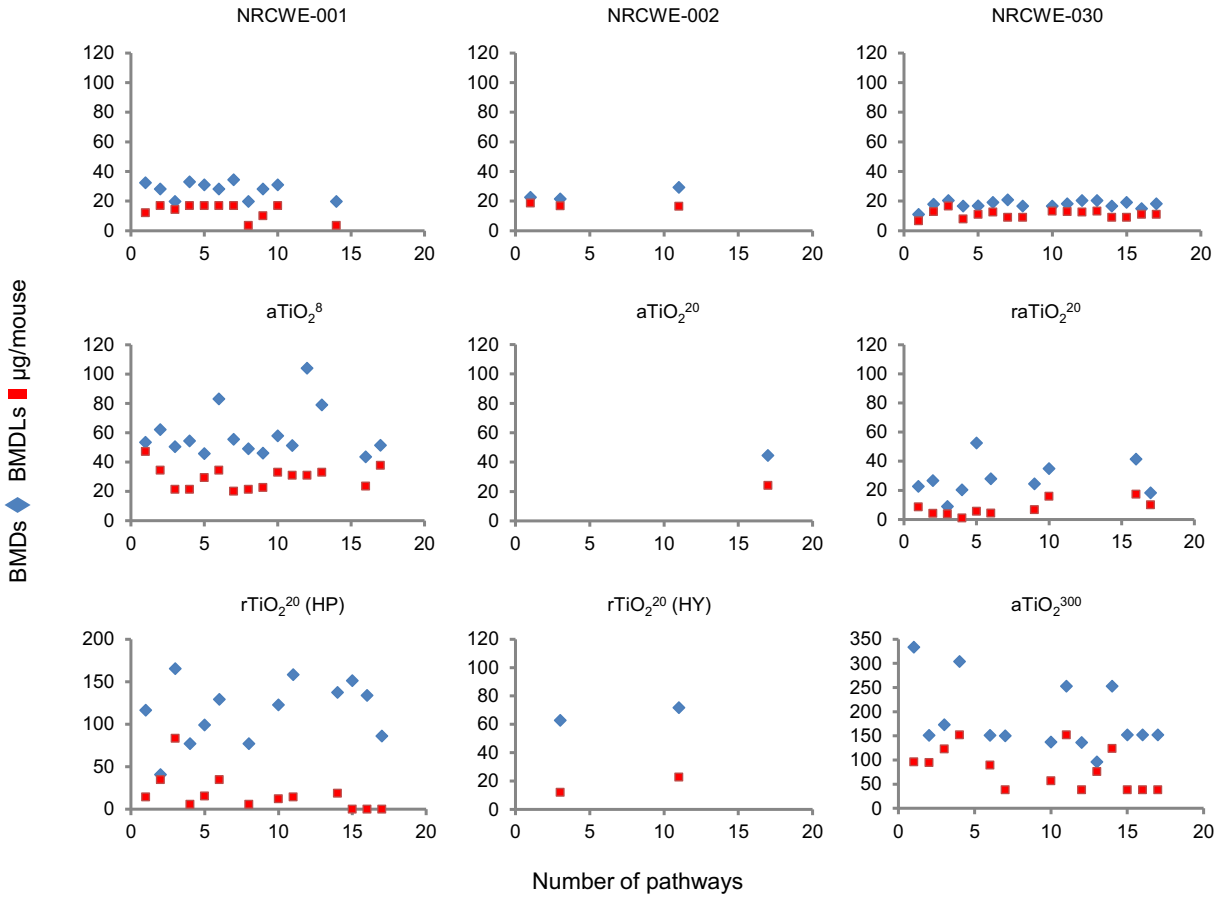

Fig. 2. Twenty most significant IPA pathways that were enriched in at least three of the nano TiO_2 exposure groups and the associated BMD/BMDL (µg/mouse) values. Any pathway with FDR p value of < 0.05 was considered significant.

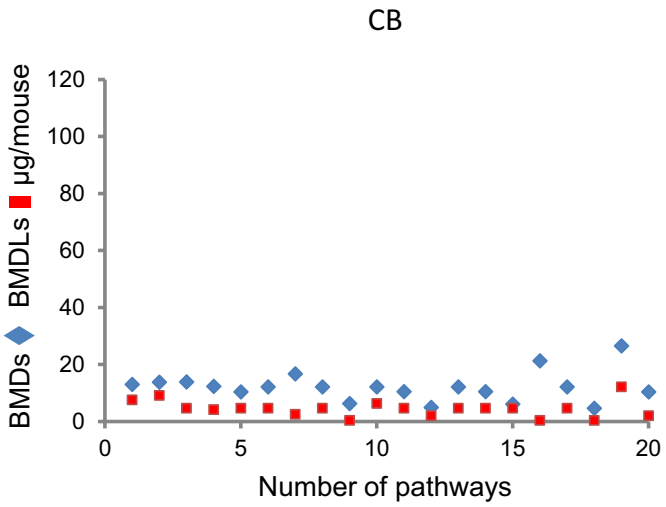

Fig. 3. Twenty most significant IPA pathways that were enriched in the CB exposure group and the associated BMD/BMDL (µg/mouse) values. Any pathway with FDR p value of < 0.05 was considered significant.

shifting the two apparent high potency TiO_2 NMs ($raTiO_2^{20}$, $rTiO_2^{20}$ (HP)) to much less potency. On the other hand, most of the TiO_2 NMs were less potent than the majority of the MWCNTs. When BMD-SA was considered (Figs. 7–9), a similar potency pattern resulted from approach 1 (Fig. 7). The BMD-SA values were scattered widely, with $raTiO_2^{20}$ and $rTiO_2^{20}$ (HP) being the high potency nano TiO_2 types and with $aTiO_2^8$ being the least potent. However, when multiple pathways with different BMD values were considered in BMD-SA (Figs. 8–9), all nano TiO_2 were aligned in a very narrow range, suggesting no potency differences between the various types, except for $aTiO_2^{20}$ and $aTiO_2^8$, which showed significantly lower potency compared to the rest.

For CB, TREM1 signaling pathway was the most sensitive pathway that showed the lowest BMD value. CB showed lower potency than NM-401 in inducing the pathway perturbations but was similar to the other MWCNT types. BMD-M or BMD-SA estimates for CB did not change much across the different approaches applied (Figs. 4–6 and 7–9).

Comparison of BMD-M and BMD-SA values for each approach showed high correlation between the two for approach 1 (r = 0.45) and less concordance with approaches 2 (r = 0.33) and 3 (r^2 = 0.30).

3.1.6. *Quantitative comparisons of potencies across NMs*

The transcriptomic responses were also assessed quantitatively in terms of the potency of NM to induce pathway perturbations. Box and whisker plots show the dose in terms of mass (Figs. 4–6) or surface area (Figs. 7–9), at which most transcriptional pathways are activated. The precision of median pathway BMD estimate were determined by plotting the potencies across the NM types with due considerations of uncertainty in the quality of experiments. The potency differences were considered significant if pathway BMD 10% and 90% confidence intervals between the NM types were non-overlapping or if they lie in a relatively narrow BMD range. Thus, it can be concluded that the confidence intervals for MWCNTs were very small (except for NRCWE-026 and NM-401) and, both BMD-M and BMD-SA values showed similar trends. Three potency classes could be identified: (1) less potent NMs showing BMD-M and BMD-SA in the range of 9–36 µg/mouse and 9–36 cm^2/mouse (Figs. 6 and 9) comprising the majority of the NMs investigated here with a few exceptions depending on mass- or surface

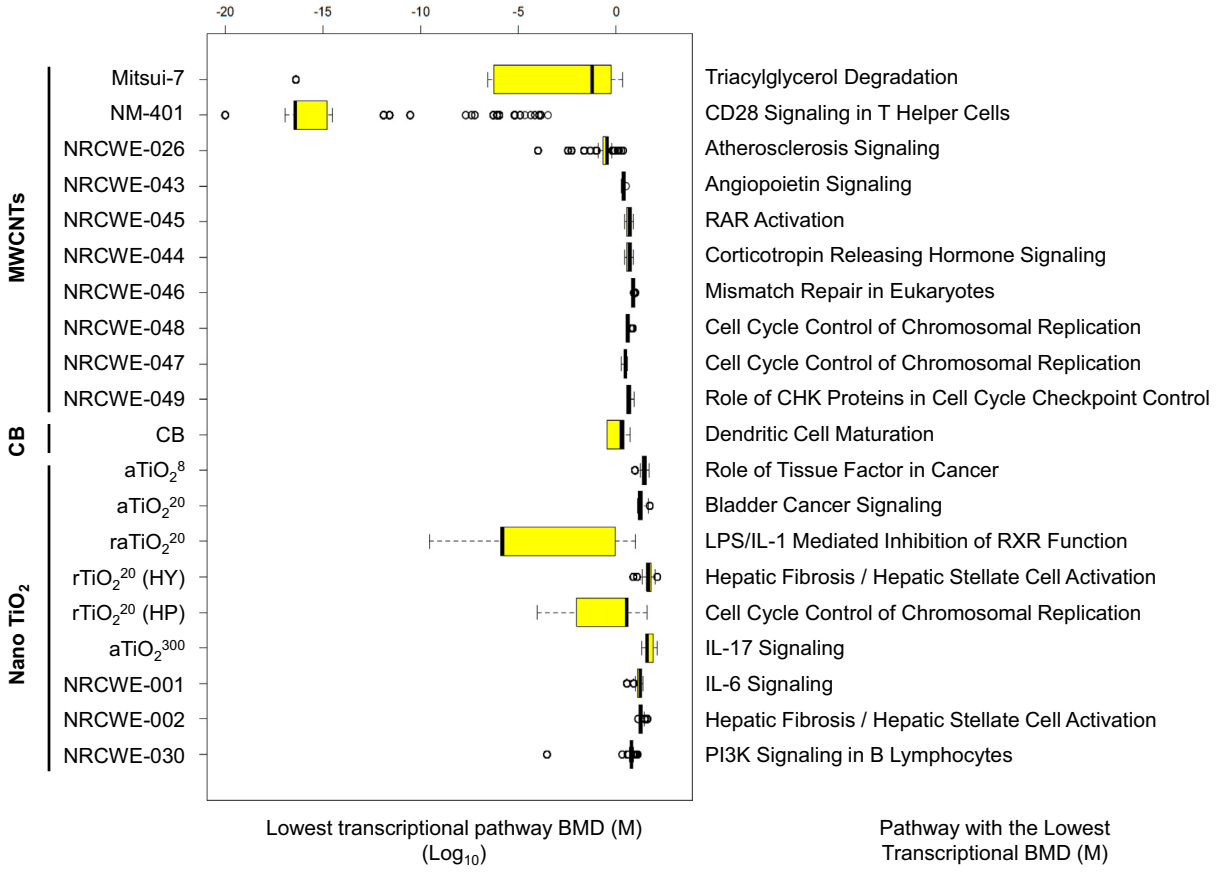

Fig. 4. Box-and-whisker plot of the most significant pathway with the lowest transcriptional BMD-M estimate for each NM type. The vertical black lines within the box plot represent medians. Box boundaries represent the interquartile ranges and the whiskers represent 10th and 90th percentiles. The pathways showing the lowest transcriptional BMD-M estimate for each NM type are listed by the side.

area-based BMD. (2) NM-401 as the high potency NM and, $aTiO_2^{8}$, $rTiO_2^{20}$ (HY), and $aTiO_2^{300}$, as low potency NMs by BMD-M (Fig. 6), and (3) NM-401 and Mitsui-7 as the high potency NMs and $aTiO_2^{8}$ and $aTiO_2^{20}$ as low potency NMs by BMD-SA (Fig. 9). Although both BMD-M and BMD-SA were comparable in potency stratification of NMs, surface area provided better agreement between BMD-SA values of less potent NMs for both approach 2 and approach 3 (Figs. 8–9) than mass (Figs. 5–6). BET surface area correlates inversely with diameter and therefore indirectly with shape. The thick MWCNTs (NM-401, Mitsui-7) showing higher potency (lower BET surface area) are more straight, stiff and needle-like than the less potent thin MWCNTs (Knudsen et al., 2018; Poulsen et al., 2016). NRCWE-026 was the exception, which showed significantly higher BMD-M/BMD-SA estimates (lower potency) when median BMD of all pathways (approach 2) was considered. Interestingly, spherical CB behaved the same as most of low potency MWCNTs and some of nano TiO_2 types. The confidence intervals were relatively large for most of nano TiO_2 types, implying data variability. In the approach considering the most sensitive pathway with the lowest pathway BMD-M/BMD-SA (approach 1), $raTiO_2^{20}$ and $rTiO_2^{20}$ (HP) were mostly non-overlapping with other nano TiO_2 types, implying that these TiO_2 types had significantly higher potency to induce pathway perturbations. However, this ranking was not preserved when median BMD-M/BMD-SA of all pathways (approach 2) was considered and for BMD-SA, no significant differences were observed among the nano TiO_2 types (except for $aTiO_2^{8}$, Fig. 8). When pathway BMD-M were analysed in cumulative fashion, NM-401 stood out as a single most potent NM to induce pathway perturbations. Steep slopes with low average BMD-M values were considered more potent than lines with flat slopes with higher BMD-M (Fig. 10).

3.2. Comparison of transcriptional BMDs with an apical BMD for lung neutrophil influx

The BMD-M values for neutrophil infiltration (BMDneu), a marker of lung inflammation, were obtained as described in the Methods section. The transcriptional BMD-M and BMDL-M values (BMDt) from each of the three approaches for each NM type were compared with the corresponding BMD/BMDLneu in BALF. Comparison of BMDneu-M values to the BMDt-M of the most sensitive pathways (approach 1) showed some concordance between the apical and transcriptional approaches (BMD-M/r = 0.36, BMD-SA/r = 0.31). The predictive power of the BMDt-M for the BMDneu was somewhat similar for approach 2 (BMD-M/r = 0.34, BMD-SA/r = 0.23) and 3 (BMD-M/r = 0.37, BMD-SA/r = 0.24). Mostly, up to a 10-fold difference was observed between the transcriptional and neutrophil BMD-M estimates, with neutrophil influx being more sensitive showing lower BMD-M than transcriptomics BMDs (Fig. 11a and b). BMDneu values for CB and NRCWE-030 were lower than the lowest dose tested and as a result did not follow the same trend as the rest. This could be the result of inappropriate dose-spacing. Since the BMDneu values for these two particle types were orders of magnitude different from the BMDneu values for the rest of particle types, they were considered outliers and removed from the correlation plot.

4. Discussion

4.1. Pathway selection for potency estimation

The guidelines for incorporating the transcriptomics data into regulatory decision making are emerging. There is interest in applying

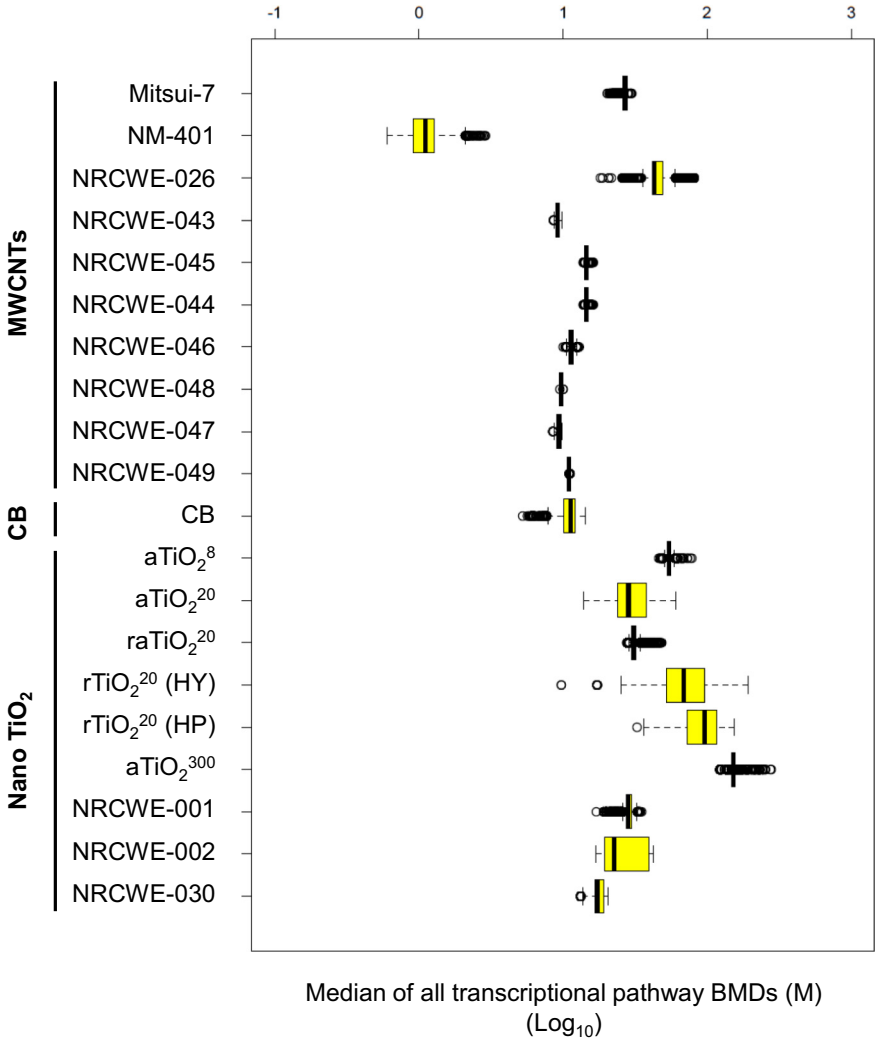

Fig. 5. Box-and-whisker plot of the median transcriptional BMD-M of all pathways for which BMD could be estimated. The vertical black lines within the boxes plot represent medians. Box boundaries represent the interquartile ranges and the whiskers represent 10th and 90th percentiles.

quantitative transcriptomics data to derive BMDs, PODs and transcriptional reference doses, in support of human health risk assessment. The present study explored if 1) transcriptional BMDs can be used to rank the potency of NMs to induce pathway perturbations indicative of *in vivo* inflammatory lung responses and 2) how predictive the absolute values of transcriptional BMDs are for inflammatory BMDs.

Transcriptomics data from mice 24 h after NM exposure were treated as continuous endpoint and the dose-response relationships were established for individual genes using conventional benchmark dose methods. The individual genes showing dose-responses were mapped to known pathways and the resulting pathway BMDs were used for rank-ordering the NMs for their potential to induce pathway perturbations associated with *in vivo* lung inflammatory responses. Three different approaches were used to select pathway BMDs for potency estimation. In addition to the mass-based BMD estimates (BMD-M), BMDs were also normalized to surface area (BMD-SA), a known predictor of particle-induced inflammation (Schmid and Stoeger, 2016; Poulsen et al., 2016). The results were compared with the apical BMDneu estimated for *in vivo* BALF neutrophil influx from the same animals.

In approach 1, the most sensitive pathway showing the lowest BMD estimate differed for each NM type. The BMDt-M derived from this approach closely aligned with the apical BMDneu-M both in terms of agreement between ranking-orders (88.2%) and absolute BMD-M values agreeing on average within a factor of 2 (slope of *ca.* 0.5 in Fig. 11a and b). The pathways included in this approach were triacylglycerol degradation, atherosclerosis signaling, angiopoietin signaling, corticotropin releasing hormone signaling and others (Figs. 4 and 6). The protein products of a few of the genes associated with these pathways are known acute phase reactants (APRs) and the specific genes that showed dose-response included 1-acylglycerol-3-phosphate O-acyltransferase (2, 3, 5) genes, lipin-2, phosphatidic acid phosphatase type 2A, inositol 1,4,5-triphosphate receptor 1, IL2-inducible T-cell kinase, matrix metallopeptidase 3, interleukin 33, selectin (platelet), and angiopoietin 1, aldehyde dehydrogenase family 1, subfamily A3, and cyclin-dependent kinase inhibitor 1A (P21), and several others. Acute phase signaling pathway is indeed upstream of the neutrophil influx event and is part of the molecular initiating event (MIE), recording the first interaction between NM and the surrounding microenvironment (Lu et al., 2010). Consequent to the MIE, danger signals/alarmins/acute phase reactants are released, initiating the acute immune response cascade involving other key events, such as the synthesis and secretion of pro-inflammatory mediators and recruitment of pro-inflammatory cells into the lungs (Labib et al., 2016b; Brockmeier et al., 2017; Nikota et al., 2017; AOP 173, OECD, 2018). Thus, at the molecular/transcriptional level, the most sensitive pathways with the lowest BMD-M estimate are indicative of upstream events that regulate influx of pro-inflammatory cells including neutrophils into the lungs,

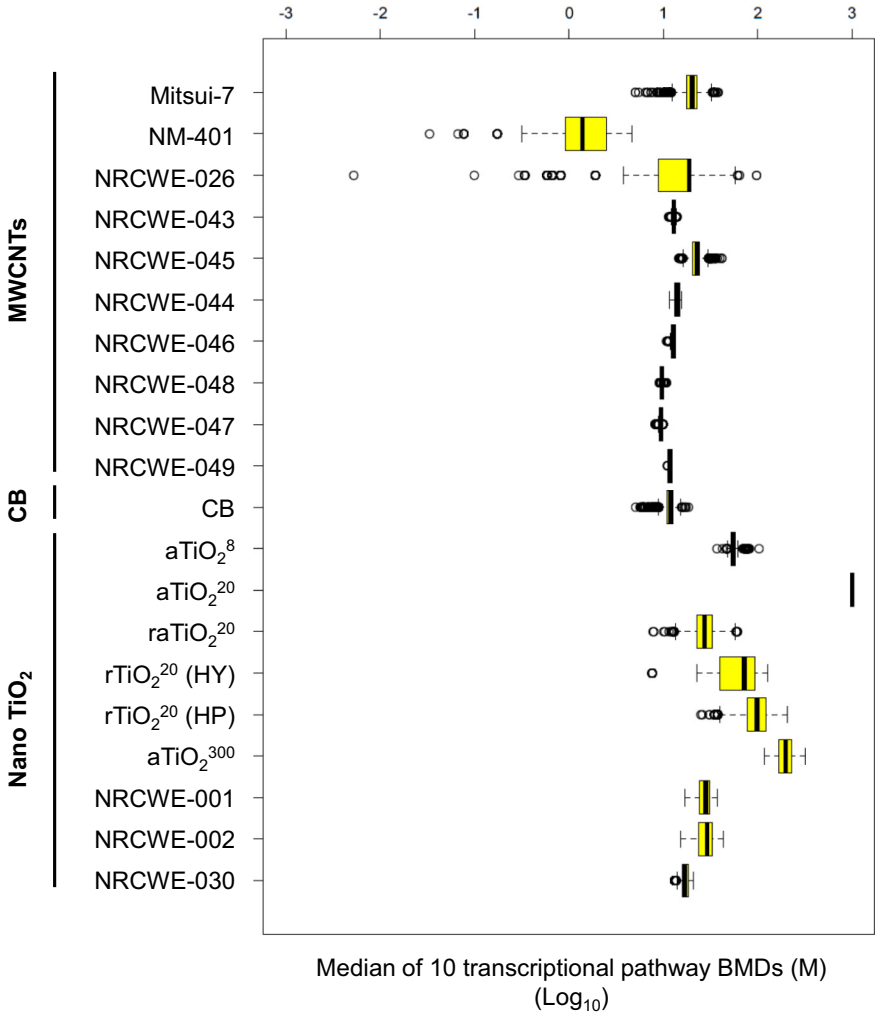

Fig. 6. Box-and-whisker plot of the median transcriptional BMD-M of 10 significant pathways commonly enriched in all three NM groups. The vertical black lines within the boxes plot represent medians. Box boundaries represent the interquartile ranges and the whiskers represent 10th and 90th percentiles. The 10 pathways are described in the Results section.

which is the first manifested and a recommended measurement in *in vivo* for inflammation quantification (Oberdoerster et al., 2005; Sayes et al., 2007). These results are in alignment with those reported by Chen et al. (2016); the study showed that carbon nanoparticle-induced neutrophil influx reached its peak at 24 hr post-exposure; whereas, peak for gene expression changes occurred at 12 h. As a result, one could argue that the gene expression and pathway alterations observed at 24 hr post-exposure could closely represent those changes that were upstream of the neutrophil influx and sustained over time. This suggests that the most sensitive pathways with the lowest BMD values reflect changes occurring at one particular time frame (24 hr post-exposure) or those that are sustained over time and do not necessarily mean that they are the first ones to be perturbed.

In a previous study, Labib et al. (2016b) applied BMD modelling to transcriptomics data and derived transcriptional PODs for MWCNT-induced lung fibrosis based on two approaches: (1) AOP-dependent approach - considering the specific pathways relevant to key events in the AOP established for MWCNT-induced lung fibrosis and, (2) AOP-independent approach (similar to what was applied in the present study) – considering any pathway exhibiting the lowest BMD value or median of all pathways for which BMDs could be estimated. The AOP-dependent approach with pathway BMDs associated with key events in the AOP more closely corresponded with the NIOSH-derived apical PODs that were based on the histopathological observation demonstrating alveolar thickness for MWCNT-induced lung fibrosis (Labib et al., 2016b). The PODs derived using AOP-independent approaches, such as the lowest BMD of a most sensitive pathway or median BMD of all pathways were either too conservative or too liberal (Labib et al., 2016b), which is the opposite to what is observed in the present study. These results may imply that the strategies to select pathways for POD determination should take into consideration the *in vivo* apical endpoint that the study is trying to predict using the transcriptomics data. While BMDs from the most sensitive pathways perturbed at 24 h were more closer to the BMDs estimated for neutrophil influx measured at 24 h in the present study, which is an acute key event in the AOP occurring immediately after NM exposure, the pathway BMDs associated with later key events in the AOP for MWCNT-induced lung fibrosis (Labib et al., 2016b) were more closer to the apical BMDs estimated for alveolar thickness, an event indicative of clinical manifestation of the fibrotic disease (Labib et al., 2016b). The AOP-independent approach or approach 1 (most sensitive pathway with the lowest BMD value) in the present study is considered conservative and supports the existing mechanistic knowledge. It also identifies novel aspects of the underlying toxicity mechanisms. It enables testing of new NMs using transcriptomics in a non-hypothesis driven manner as it does not require *a priori* understanding of the NM mode-of-action. This is important as the underlying mechanisms of toxicity for most NMs are not known. Based on this approach, considering the median (BMD-M or BMD-SA), the

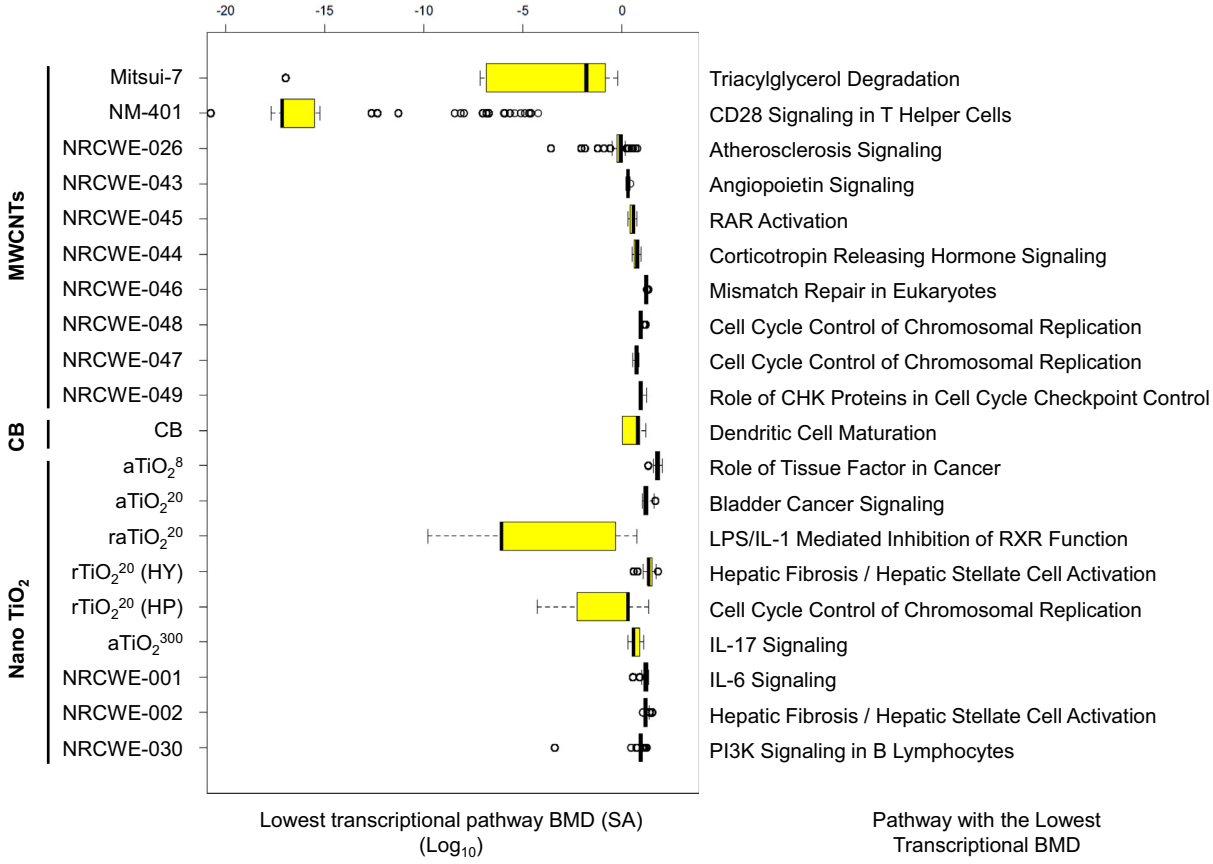

Fig. 7. Box-and-whisker plot of the most significant pathway with the lowest transcriptional BMD-SA estimate for each NM type. The vertical black lines within the boxes plot represent medians. Box boundaries represent the interquartile ranges and the whiskers represent 10th and 90th percentiles. The pathways showing the lowest transcriptional BMD-SA estimate for each NM type are listed by the side.

potency of NMs to induce pathway perturbations could be ranked as NM-401$^{>}$ raTiO$_2^{20}$ $^{>}$ Mitsui-7 $^{>}$ NRCWE-026 $^{>}$ NRCWE-043 -049/CB/ rTiO$_2^{20}$(HP) $^{>}$other nano TiO$_2$. Among the nano TiO$_2$, raTiO$_2^{20}$ was clearly the most potent; however, the BMDs for the rest of the nano TiO$_2$ types were very similar. This may imply that all the assessed TiO$_2$ NMs could be grouped under the same bin. The results of approach 1 were most correlative (BMD-M r = 0.36, BMD-SA r = 0.31) to the apical neutrophil influx BMDs. For most MWCNT types and nano TiO$_2$, the transcriptional BMDs remained within 10-fold of the apical BMDs.

In approach 2 (median BMD of all pathways), all pathways with BMD estimates were included. This approach resulted in pathway BMDs that were higher but within the 10-fold difference from approach 1. Similar to approach 2, consideration of 10 most significant pathways that were common across the three NM groups in approach 3 resulted in larger median pathway BMDs. Approach 3 is mechanistically supportive of the biology perturbed; a majority of the pathways included in this approach were associated with the observed acute neutrophil influx and the lung immune response. Some of the genes associated with these pathways are measured *in vivo* or in *in vitro* assays as markers of lung inflammation. However, the results of the approaches 2 and 3 were similar to approach 1 when BMD-M was considered and less concordant with the BMD-SA; approach 2 (BMD-M r = 0.34, BMD-SA r = 0.23) and 3 (BMD-M r = 0.37, BMD-SA r = 0.24). Transcriptional BMDts were larger (10-fold difference) than the BMDs for neutrophil influx. The reasons for this lack of concordance could be that the genes involved are not the initiators of neutrophil influx, rather the downstream effectors of the induced neutrophil influx or those that are secreted by the neutrophils themselves. Approach 2 ranked NM-401 as the most potent and NRCWE-026 as the least potent of all MWCNT types. There was no clear distinction among the nano TiO$_2$ types. The results of approach 3 were much similar to approach 2. In general, the results of BMD-M were in agreement with those of BMD-SA. Thus, based on the pathways used, the PODs may differ. Several studies have applied BMD modelling to assess the transcriptional dose response relationships and have demonstrated that transcriptional PODs agree with the PODs derived using apical endpoints (Bercu et al., 2010; Labib et al., 2016b; Thomas et al., 2007; Moffat et al., 2015). However, there are no standardised protocols or guidance available for selecting specific genes or pathways used to determine the PODs. In the present study, of the three approaches, approach 1 – consideration of a pathway with the lowest transcriptional BMD value, showed higher correlation with the apical BMDs, and thus, is a recommended approach for selecting pathways in support of POD calculation. However, how the processes for selecting pathways and the resulting differences in BMDs will impact the overall decision making process is yet to be determined.

Regardless of the approach used, most MWCNTs showed tighter BMD distribution with the exception of NRCWE-026. Large interquartile ranges were observed for most nano TiO$_2$ types in all three approaches, suggesting high data variability. NRCWE-025, a 38 nm rutile nano TiO$_2$ was excluded from the analysis entirely since there were no significantly enriched IPA pathways, for which BMDs could be calculated. Also, approach 3 could not be applied to aTiO$_2^{20}$ as none of the 10 pathways used were present in this group. Moreover, a gene that did not show dose response or a pathway that has < 5 probes were also not included in the analysis, limiting its application to deriving broader conclusions. Also, the analysis was limited to statistically significant and differentially expressed genes. However, it is important to note that the overall dose-response of pathways may be independent of single genes. These results show the limitations of the transcriptional BMD approach in general and also reflect some of the limitations of the

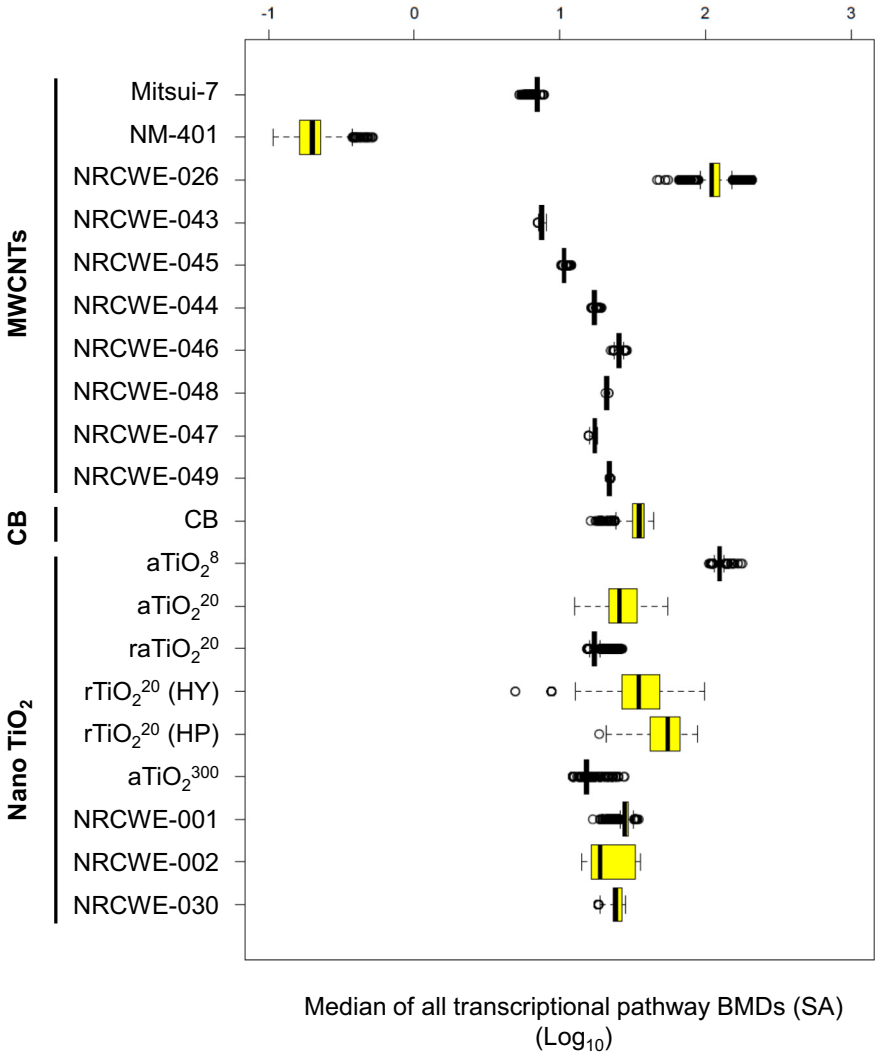

Fig. 8. Box-and-whisker plot of the median transcriptional BMD-SA of all pathways for which BMD could be estimated. The vertical black lines within the boxes plot represent medians. Box boundaries represent the interquartile ranges and the whiskers represent 10th and 90th percentiles.

approaches used in the present study.

Albeit the many limitations, in general, the results are largely in agreement with the published literature. The Mitsui-7 and NM-401, have been shown to induce similar acute inflammatory responses in mice following single intratracheal instillation. A study involving repeated intratracheal instillation of Mitsui-7 or NM-401 in mouse lungs showed higher collagen deposition 60-days post-exposure in mice exposed to NM-401 compared to mice exposed to Mitsui-7 (Rahman et al., 2017). Among the nano TiO_2 types, the mixed rutile/anatase 20 nm nano TiO_2 has been known to be more potent than the other variants of nano TiO_2 types. *In vivo*, exposure to high doses of $raTiO_2^{20}$ or $rTiO_2^{20}$ (HP) induced higher lung inflammation and increased collagen deposition at 28 days post-exposure compared to the other nano TiO_2 types (Rahman et al., 2016). These results suggest that transcriptomics data can be used to rank the toxic potency of NM in the absence of data from the standardised tests.

4.2. NM physico-chemical characteristics and influence on potency estimation

It is suggested that NM-induced toxicity is driven by their diverse physico-chemical properties (Knudsen et al., 2018; Poulsen et al., 2017). The physical properties of MWCNTs including the length, diameter and rigidity influence their toxicity. In addition, metal contaminants, surface charge and surface functionality (surface functionalization with small organic molecules such as carboxyl or hydroxyl groups) are suggested to contribute to the reactivity, stability, and dispersability, thereby influencing their toxicity potential. However, existing data from animal experiments have shown inconsistent results; for example, in several studies, mice exposed to pristine or carboxylated MWCNTs showed reduced lung immune and pathologic response, and in (Poulsen et al., 2016; Hamilton et al., 2013; Sager et al., 2014) other studies, carboxylation of MWCNTs was shown to increase or not alter the lung responses in mice compared to the responses induced by pristine MWCNTs (Dandley et al., 2015; Patlolla et al., 2010; Ursini et al., 2016).

The individual MWCNTs (NRCWE-043 – NRCWE-049) assessed in the present study varied in length (average length of 750–1500 nm), diameter (diameter of 26 nm–32 nm), oxygen content (NRCWE -044 and NRCWE - 045 showed higher oxygen content compared to NRCWE-043) (Poulsen et al., 2016; Jackson et al., 2015b). In addition, metal contaminants including Fe_2O3, CoO, NiO, MgO and MnO were found to a varying degree; NRCWE-043, NRCWE-044, and NRCWE-045 showed relatively more Ni and Fe content than others. NRCWE-046 – NRCWE-049 contained more Al, Co and Mg contaminants. Of the contaminants, iron levels showed a high level of variability across the MWCNT types. The other MWCNTs varied in their diameter; Mitsui-7 (74 nm in diameter), NM-401 (67 nm in diameter) and NRCWE-026 (10 nm

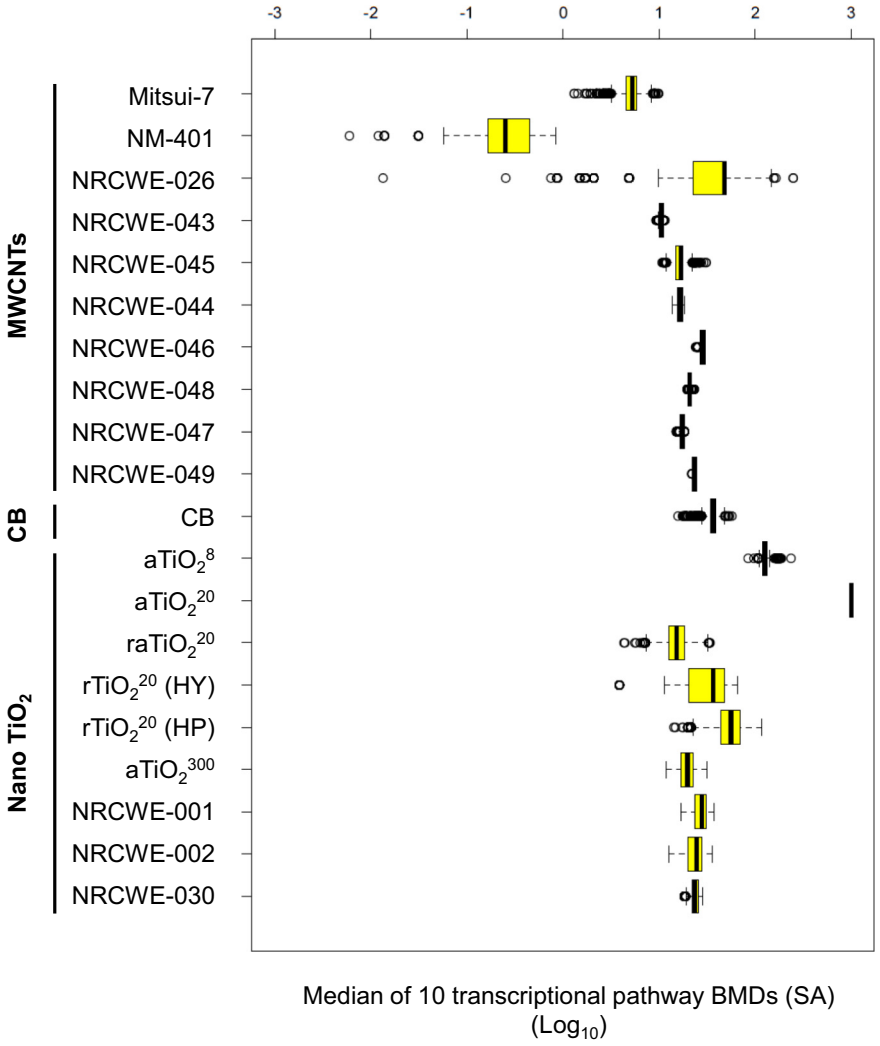

Fig. 9. Box-and-whisker plot of the median transcriptional BMD-SA of 10 significant pathways commonly enriched in all three NM groups. The vertical black line within the box plot represents medians. Box boundaries represent the interquartile ranges and the whiskers represent 10th and 90th percentiles. The 10 pathways are described in the Results section.

diameter). However, the BMD dose-response modelling and potency estimation did not show large differences between the MWCNT types with the exception of NM-401 and Mitsui-7, especially when BMD-SA is considered. The pathway BMD values for Mitsui-7 and NM-401 were very similar and ranged from 1.4 μg/mouse to 11.6 μg/mouse, which were much lower compared to the other MWCNTs (NM -043 – NM-049). However, pathway BMD values for NRCWE-026 were very large and varied from 7.1 μg/mouse to 131.1 μg/mouse. Mitsui-7 and NM-401 are long and rigid tubes that have been consistently shown to induce lung fibrotic response in rodents (Poulsen et al., 2015; Nikota et al., 2017; Rahman et al., 2017). NRCWE-026 is a long tangled tube, which is shown to induce more inflammation and acute phase response but less fibrosis compared to NM-401 (Poulsen et al., 2015). The MWCNTs NRCWE-043 – NRCWE-049 have diameters in the range of 13–26 nm and are therefore more comparable to NRCWE-026 (diameter 10 nm) than to Mitsui-7 and NM-401 exhibiting diameters of 74 nm and 67 nm, respectively.

The results are in alignment with published reports for various types of MWCNTs; repeated intratracheal exposure to high doses of Mitsui-7 or NM-401 resulted in quantifiable lung fibrosis in mice (Rahman et al., 2017). The thick and rigid MWCNT Mitsui-7 is the only MWCNT which is classified as possibly carcinogenic and has been shown to induce lung cancer by inhalation (Kasai et al., 2015). Subsequently, four other thick and long MWCNTs were shown to induce adenomas after intra peritoneal exposure (Rittinghausen et al., 2014). In a recent study of long-term histopathological effects following MWCNT exposure, the thick NM-401 and Mitsui-7 were found distributed as single fibres in lung tissue one year after exposure, whereas the thinner MWCNTs were observed as aggregates in granulomas and macrophages (Knudsen et al., 2018). These results suggest that the tissue distribution and aggregation status of the fibres may contribute to their toxicity. In another recent study, lung immune and genotoxic responses were investigated at different post-exposure time points following exposure of mice to various doses of thin, thick or short MWCNTs of pristine surface or MWCNTs functionalized with carboxyl (COOH), hydroxyl (OH) or amine (NH_2) groups, that included NRCWE-043 – NRCWE-049. The study concluded that MWCNT-induced lung inflammation was positively associated with deposited surface area, whereas genotoxicity was influenced by the tube diameter (Poulsen et al., 2016; Jackson et al., 2015b). Based on the results from the studies described above and from the results of the present study, it can be concluded that (1) some MWCNT properties influence the acute lung responses; however the underlying mechanisms of toxicity are the same regardless of the different properties, (2) the expression of several genes involved in these pathways are altered at very low doses and (3) the progress towards an adverse outcome may be determined by the specific material properties,

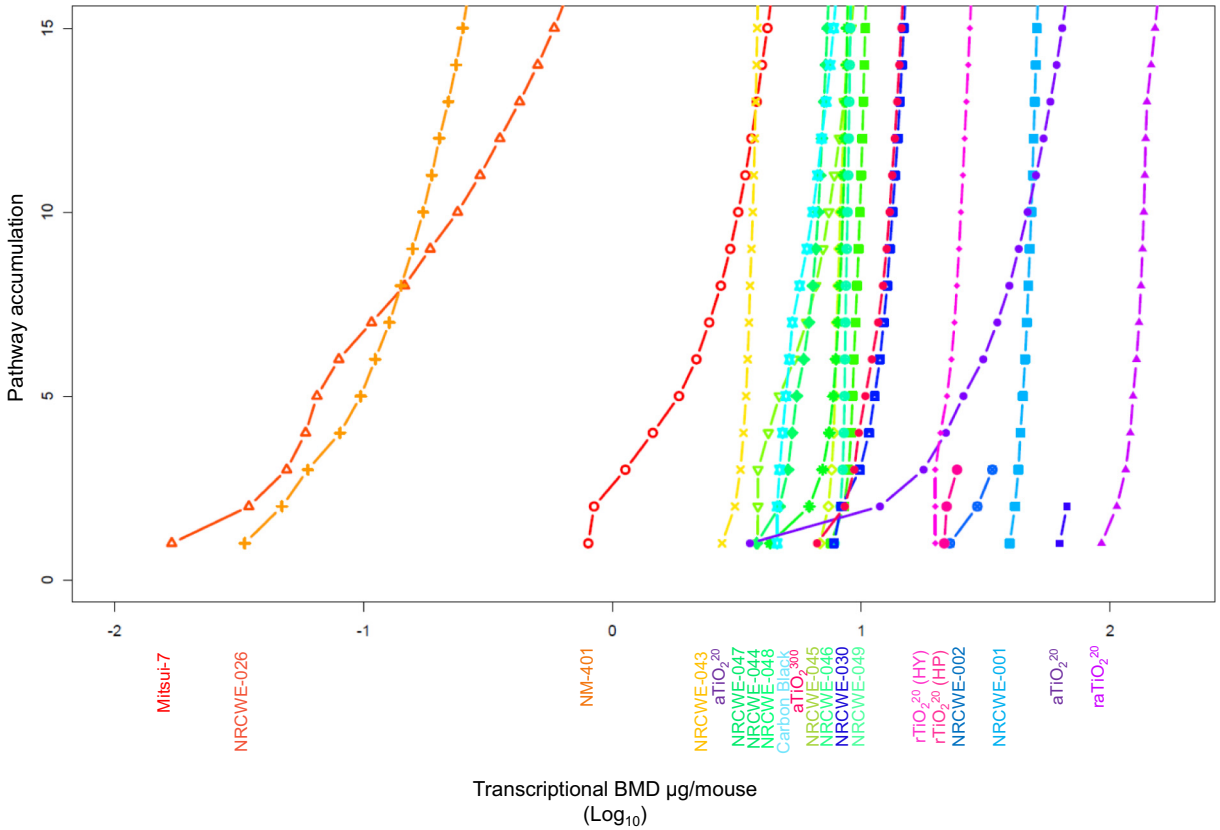

Fig. 10. A pathway accumulation plot for each NM type. The y-axis represents the number of pathways used to estimate the average pathway BMD-M and the x-axis represents the average BMD. Each NM is represented by a line in the plot and individual NM types are listed on the side with the corresponding colour. (For interpretation of the references to colour in this figure legend, the reader is referred to the web version of this article.)

duration of exposure, biopersistence and post-exposure time.

For nano TiO_2, primary particle size, shape, crystalline structure, and surface charge are suggested to be the factors impacting their toxicity (Warheit et al., 2007; Sweeney et al., 2015). In the present study, the particle size for nano TiO_2 varied from 8 to 38 nm with a larger bulk TiO_2 type exhibiting 300 nm size. They belonged to anatase, rutile or mixed anatase/rutile crystalline structure, and exhibited different surface properties. Pathway BMDs were calculated for all TiO_2 types except for the 38 nm NRCWE-025, which showed no pathways perturbed at the assessed dose levels. Although there was no clear potency distinction between the various nano TiO_2 types, the mixed $raTiO_2^{20}$ and $rTiO_2^{20}$(HY) could be considered as more potent than the other rutile and anatase types of TiO_2 of 20 nm size by approach 1 (pathway BMD of most sensitive pathway with the lowest BMD value), suggesting that the crystalline structure and hydrophobic surface could be the properties contributing to the effects. Previous studies have shown that intratracheal instillation of mixed (80/20 anatase/rutile) nano TiO_2 induced 40 times more pulmonary inflammation and lung damage than an equal mass dose of 100% rutile forms of nano TiO_2 (Sager et al., 2008). Mice lungs exposed to high doses of mixed $raTiO_2^{20}$ or $rTiO_2^{20}$(HY) presented with higher collagen deposition in lungs compared to other anatase type nano TiO_2 or $rTiO_2^{20}$(HP), suggesting that specific surface modifications render them more toxic (Rahman et al., 2016). However, the potency ranking of nano TiO_2 widely differed based on the approaches used. Unlike for MWCNTs, the confidence intervals for nano TiO_2 were large except for NRCWE-001, 002 and 030, which are 10 nm rutile types. The present study did not reveal size specific trends in toxicity induced by nano TiO_2 types.

4.3. Relevance to in vitro study designs

The present study used *in vivo* mouse lung transcriptomics data for determining the potency of various NM to induce *in vivo* lung inflammation, *i.e.* BALF neutrophil influx. Although, animal tests are integral to regulatory toxicological studies, they are time and resource intensive. Given the number and versatility of NMs that are being produced that require assessment, animal testing is not anymore an option for the vast number of them. Animal alternatives that are predictive of an outcome of regulatory relevance and can provide information on exposure concentrations at which the effects occur, are highly desired. However, 'what to measure' in *in vitro* models that lack the sophistication of an intact organ involving multicellular and systemic interactions that are central to responses such as lung inflammation, is a debatable question. In general, in *in vitro* models, the inflammatory endpoint is assessed *via* measuring the expression levels of pro-inflammatory genes in specific cells and/or cytokines, chemokines and growth factors secreted in cell supernatants (Sayes et al., 2007), the selection of which is mainly based on cell types, the expertise of the individual laboratory or the researcher. Although the expression of several pro-inflammatory molecules is altered following *in vitro* exposures to NM, often, the expression levels do not show dose-dependency. This could be due to the insufficient doses that include activation and resolution points in a dose-response curve. The results from the present study can be used to help identify the appropriate markers of inflammation to measure *in vitro* and design or develop suitable *in vitro* assays. For example, inclusion of a select set of genes from the most sensitive pathways with the lowest BMD that show dose concordance with the *in vivo* neutrophil influx may help improve the sensitivity of the existing *in vitro* assays for measuring pro-inflammatory responses in lung. However, considering the simplicity of *in vitro*

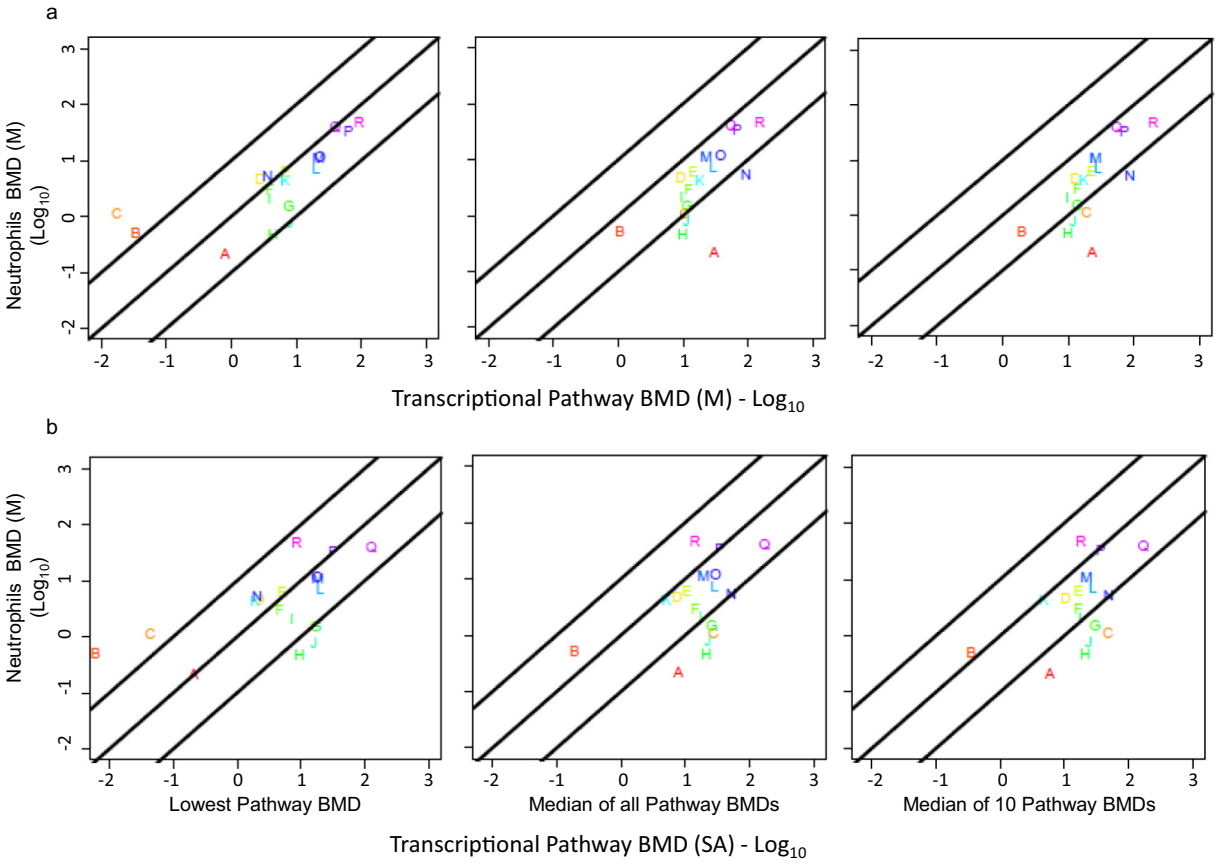

Fig. 11. a: Scatter plots showing the relationship between mass-based transcriptional BMD (BMDt) and neutrophil influx (BMDneu). Each of the 20 NMs is coloured differently. The middle black line represents equal transcriptional BMDt-M and neutrophil influx BMDneu-M values. The upper and lower black lines represent 10-fold difference between the BMD values. Correlation coefficients (*r*) are included at the top corner.
b: Scatter plots showing the relationship between surface area-based transcriptional BMD (BMDt) and neutrophil influx (BMDneu). Each of the 20 NMs is coloured differently. The middle black line represents equal transcriptional BMDt-SA and neutrophil influx BMDneu-SA values. The upper and lower black lines represent 10-fold difference between the BMD values. Correlation coefficients (*r*) are included at the top corner. (For interpretation of the references to colour in this figure legend, the reader is referred to the web version of this article.)

models and sophistication of *in vivo* organs, a direct comparison of the NM-induced responses between the two models (*in vitro vs in vivo*) may not be realistic. In that context, non-hypothesis driven or mechanisms-independent approaches such as approach 1 suggested in the present study (selecting pathways with the lowest BMD values) can be applied to transcriptomics data derived from *in vitro* animal alternatives following exposure to *in vivo* relevant doses of NMs. The results derived from such studies may be used to support similar ranking or prioritisation decisions.

5. Conclusions

A number of studies have shown that global changes in gene expression following substance exposure are related to dose, and can serve as sensitive markers of early pathophysiological change. The present study applied transcriptional dose-response modelling to rank the potency of NMs to induce pathway perturbations associated with the observed lung inflammatory responses in *in vivo* studies. The results showed that the underlying pathways of toxicity are the same for all NMs tested and that the acute toxic responses cannot be clearly distinguished by the specific phys-chem properties. Based on the transcriptional BMD estimates, it can be proposed that the long, rigid and stiff MWCNTs are definitely the high priority MWCNTs for toxicity testing; however, all MWCNTs should be prioritised and must be considered for further investigation with multiple dose and post-exposure time points. Among the nano TiO_2 types, mixed rutile/anatase type ($raTiO_2$[20]) is a high-priority TiO_2 along with hydrophilic rutile phase TiO_2 ($rTiO_2$[20](HY)). Although the transcriptional BMD-M and BMD-SA were mostly in agreement, the results show that BMD-M is much more conservative. The study also identified novel aspects of the lung acute responses to NMs and potential gene markers that may provide dose-response information for quantifying the *in vivo* lung inflammation. Inclusion of these novel genes in the panel of pro-inflammatory mediators that are assessed *in vitro* may improve the accuracy and sensitivity of the pro-inflammatory *in vitro* assays.

The desire to incorporate toxicogenomics data into human health risk assessment is impeded by the lack of internationally harmonised protocols and guidelines. Owing to hundreds and thousands of genes that show changes in expression following a toxicant exposure, the selection of genes and associated pathways that are most relevant to the observed *in vivo* response or adverse outcome is the challenge. In the present study, three individual approaches were tested. Although the choice of genes and pathways that support the known mechanisms of action or the established adverse outcome pathways is the ideal approach, for most NM classes, information on mode of action is not available. The individual approaches presented in the study include mechanism-dependent (approaches 2 and 3) and independent (approach 1) approaches supporting the use of transcriptomics data in quantitative dose-response analysis for all NMs with known and unknown mode of action. Of the three individual approaches investigated, approach 1 – consideration of the pathway with the lowest transcriptional BMD value was the consistently correlative to the apical BMDs,

with both dose metrics BMD-M and BMD-SA. Approach 1 is also the recommended approach by others for selecting pathways for POD calculation. Finally, the present study demonstrated the concordance between the transcriptional PODs and the apical PODs.

Supplementary data to this article can be found online at https://doi.org/10.1016/j.impact.2019.100158.

Funding

Funding for this work was provided by Genomics Research and Development Initiative and Chemicals Management Plan of Health Canada, Ottawa, Canada. Petra Jackson and Sarah S Poulsen received funding from the Danish Centre for Nanosafety 2 (Copenhagen, Denmark). Ulla B Vogel, Otmar Schmid and Yaobo Ding received funding from the European Union's Horizon 2020 research and innovation programme under grant agreement No. 686098 (SmartNanoTox).

Acknowledgment

Authors would like to acknowledge Dr. Nikolai Chepelev, Environmental Health Science and Research Bureau, Health Canada, Ottawa, Ontario, Canada and Dr. Kathy Nguyen, New Substances Assessment and Control Bureau, Health Canada, Ottawa, Ontario, Canada for their valuable comments on the manuscript.

References

AOP 173, OECD. (under review). In).
Benjamini, Y., Hochberg, Y., 1995. Controlling the false discovery rate: a practical and powerful approach to multiple testing. J. R. Stat. Soc. Ser. B Methodol. 289–300.
Bercu, J.P., Jolly, R.A., Flagella, K.M., Baker, T.K., Romero, P., Stevens, J.L., 2010. Toxicogenomics and cancer risk assessment: a framework for key event analysis and dose-response assessment for nongenotoxic carcinogens. Regul. Toxicol. Pharmacol. 58, 369–381.
Borm, P.J., Robbins, D., Haubold, S., Kuhlbusch, T., Fissan, H., Donaldson, K., Schins, R., Stone, V., Kreyling, W., Lademann, J., 2006. The potential risks of nanomaterials: a review carried out for ECETOC. Particle and Fibre Toxicology 3, 11–45.
Bourdon, J.A., Halappanavar, S., Saber, A.T., Jacobsen, N.R., Williams, A., Wallin, H., Vogel, U., Yauk, C.L., 2012. Hepatic and pulmonary toxicogenomic profiles in mice intratracheally instilled with carbon black nanoparticles reveal pulmonary inflammation, acute phase response, and alterations in lipid homeostasis. Toxicol. Sci. 127, 474–484.
Brockmeier, E.K., Hodges, G., Hutchinson, T.H., Butler, E., Hecker, M., Tollefsen, K.E., Garcia-Reyero, N., Kille, P., Becker, D., Chipman, K., 2017. The role of omics in the application of adverse outcome pathways for chemical risk assessment. Toxicol. Sci. 158, 252–262.
Buesen, R., Chorley, B.N., da Silva, L.B., Daston, G., Deferme, L., Ebbels, T., Gant, T.W., Goetz, A., Greally, J., Gribaldo, L., Hackermuller, J., Hubesch, B., Jennen, D., Johnson, K., Kanno, J., Kauffmann, H.M., Laffont, M., McMullen, P., Meehan, R., Pemberton, M., Perdichizzi, S., Piersma, A.H., Sauer, U.G., Schmidt, K., Seitz, H., Sumida, K., Tollefsen, K.E., Tong, W., Tralau, T., van, R.B., Weber, R.J.M., Worth, A., Yauk, C., Poole, A., 2017. Applying 'omics technologies in chemicals risk assessment: report of an ECETOC workshop. Regul. Toxicol. Pharmacol. 91 (Suppl. 1), S3–S13.
Chen, S., Yin, R., Mutze, K., Yu, Y., Takenaka, S., 2016. No involvement of alveolar macrophages in the initiation of carbon nanoparticle induced acute lung inflammation in mice. Part. Fibre Toxicol. 13, 33.
Chepelev, N.L., Long, A.S., Bowers, W.J., Gagné, R., Williams, A., Kuo, B., Phillips, D.H., Arlt, V.M., White, P.A., Yauk, C.L., 2016. Transcriptional profiling of the mouse hippocampus supports an NMDAR-mediated neurotoxic mode of action for benzo [a] pyrene. Environ. Mol. Mutagen. 57, 350–363.
Cui, X., Hwang, J.G., Qiu, J., Blades, N.J., Churchill, G.A., 2005. Improved statistical tests for differential gene expression by shrinking variance components estimates. Biostatistics 6, 59–75.
Dandley, E.C., Taylor, A.J., Duke, K.S., Ihrie, M.D., Shipkowski, K.A., Parsons, G.N., Bonner, J.C., 2015. Atomic layer deposition coating of carbon nanotubes with zinc oxide causes acute phase immune responses in human monocytes in vitro and in mice after pulmonary exposure. Particle and Fibre Toxicology 13, 29–45.
Effort, B., Tibshirani, R.J., 1993. An Introduction to the Bootstrap. Chapman and Hall, New York.
Farmahin, R., Williams, A., Kuo, B., Chepelev, N.L., Thomas, R.S., Barton-Maclaren, T.S., Curran, I.H., Nong, A., Wade, M.G., Yauk, C.L., 2017. Recommended approaches in the application of toxicogenomics to derive points of departure for chemical risk assessment. Arch. Toxicol. 91, 2045–2065.
Geraci, C.L., Castranova, V., 2010. Challenges in assessing nanomaterial toxicology: a personal perspective. Wiley Interdisciplinary Reviews: Nanomedicine and Nanobiotechnology 2, 569–577.
Grosse, Y., Loomis, D., Guyton, K.Z., Lauby-Secretan, B., El, G.F., Bouvard, V., Benbrahim-Tallaa, L., Guha, N., Scoccianti, C., Mattock, H., Straif, K., 2014. Carcinogenicity of fluoro-edenite, silicon carbide fibres and whiskers, and carbon nanotubes. Lancet Oncol 15, 1427–1428.
Haber, L.T., Dourson, M.L., Allen, B.C., Hertzberg, R.C., Parker, A., Vincent, M.J., Maier, A., Boobis, A.R., 2018. Benchmark dose (BMD) modeling: current practice, issues, and challenges. Crit. Rev. Toxicol. 48, 387–415.
Halappanavar, S., Saber, A.T., Decan, N., Jensen, K.A., Wu, D., Jacobsen, N.R., Guo, C., Rogowski, J., Koponen, I.K., Levin, M., 2015. Transcriptional profiling identifies physicochemical properties of nanomaterials that are determinants of the in vivo pulmonary response. Environ. Mol. Mutagen. 56, 245–264.
Halappanavar, S., Rahman, L., Nikota, J., Poulsen, S.S., Ding, Y., Jackson, P., Wallin, H., Schmid, O., Vogel, U., Williams, A., 2019;al., In press. Ranking of nanomaterial potency to induce pathway perturbations associated with lung responses. NANOIMPACT (In press).
Hamadeh, H.K., Bushel, P.R., Jayadev, S., Martin, K., DiSorbo, O., Sieber, S., Bennett, L., Tennant, R., Stoll, R., Barrett, J.C., 2002. Gene expression analysis reveals chemical-specific profiles. Toxicol. Sci. 67, 219–231.
Hamilton, R.F., Wu, Z., Mitra, S., Shaw, P.K., Holian, A., 2013. Effect of MWCNT size, carboxylation, and purification on in vitro and in vivo toxicity, inflammation and lung pathology. Particle and Fibre Toxicology 10, 57–75.
Heinrich, U., Fuhst, R., Rittinghausen, S., Creutzenberg, O., Bellmann, B., Koch, W., Levsen, K., 1995. Chronic inhalation exposure of Wistar rats and two different strains of mice to diesel engine exhaust, carbon black, and titanium dioxide. Inhal. Toxicol. 7, 533–556.
Husain, M., Saber, A.T., Guo, C., Jacobsen, N.R., Jensen, K.A., Yauk, C.L., Williams, A., Vogel, U., Wallin, H., Halappanavar, S., 2013. Pulmonary instillation of low doses of titanium dioxide nanoparticles in mice leads to particle retention and gene expression changes in the absence of inflammation. Toxicol. Appl. Pharmacol. 269, 250–262.
IARC monographs on the evaluation of carcinogenic risks to humans: carbon black, titanium dioxide, and talc. In: IARC Working Group on the Evaluation of Carcinogenic Risk to Humans. International Agency for Research on Cancer.
Jackson, P., Kling, K., Jensen, K.A., Clausen, P.A., Madsen, A.M., Wallin, H., Vogel, U., 2015a. Characterization of genotoxic response to 15 multiwalled carbon nanotubes with variable physicochemical properties including surface functionalizations in the FE1-Muta(TM) mouse lung epithelial cell line. Environ. Mol. Mutagen. 56, 183–203.
Jackson, P., Kling, K., Jensen, K.A., Clausen, P.A., Madsen, A.M., Wallin, H.+., Vogel, U., 2015b. Characterization of genotoxic response to 15 multiwalled carbon nanotubes with variable physicochemical properties including surface functionalizations in the FE 1GÇÉMuta (TM) mouse lung epithelial cell line. Environ. Mol. Mutagen. 56, 183–203.
Johnston, H., Pojana, G., Zuin, S., Jacobsen, N.R., Møller, P., Loft, S., Semmler-Behnke, M., McGuiness, C., Balharry, D., Marcomini, A., 2013. Engineered nanomaterial risk. Lessons learnt from completed nanotoxicology studies: potential solutions to current and future challenges. Crit. Rev. Toxicol. 43, 1–20.
Kasai, T., Umeda, Y., Ohnishi, M., Mine, T., Kondo, H., Takeuchi, T., Matsumoto, M., Fukushima, S., 2015. Lung carcinogenicity of inhaled multi-walled carbon nanotube in rats. Particle and Fibre Toxicology 13, 53.
Kasai, T., Umeda, Y., Ohnishi, M., Mine, T., Kondo, H., Takeuchi, T., Matsumoto, M., Fukushima, S., 2016. Lung carcinogenicity of inhaled multi-walled carbon nanotube in rats. Part Fibre Toxicol 13, 1–19.
Knudsen, K.B., Berthing, T., Jackson, P., Poulsen, S.S., Mortensen, A., Jacobsen, N.R., Skaug, V., Szarek, J., Hougaard, K.S., Wolff, H., 2018. Physicochemical predictors of multi-walled carbon nanotube-induced pulmonary histopathology and toxicity one year after pulmonary deposition of 11 different multi-walled carbon nanotubes in mice. Basic Clin Pharmacol Toxicol 124 (2), 211–227.
Kohonen, P., Parkkinen, J.A., Willighagen, E.L., Ceder, R., Wennerberg, K., Kaski, S., Grafström, R.C., 2017. A transcriptomics data-driven gene space accurately predicts liver cytopathology and drug-induced liver injury. Nat. Commun. 8, 15932.
Kreyling, W.G., Scheuch, G., 2000. Clearance of particles deposited in the lungs. Lung Biology in Health and Disease. 143. pp. 323–376.
Kreyling, W.G., Semmler-Behnke, M., Seitz, J., Scymczak, W., Wenk, A., Mayer, P., Takenaka, S., Oberdoerster, G., 2009. Size dependence of the translocation of inhaled iridium and carbon nanoparticle aggregates from the lung of rats to the blood and secondary target organs. Inhal. Toxicol. 21, 55–60.
Kreyling, W.G., Hirn, S., Möller, W., Schleh, C., Wenk, A., Celik, G., Lipka, J., Scha¦êffler, M., Haberl, N., Johnston, B.D., 2013. Air-blood barrier translocation of tracheally instilled gold nanoparticles inversely depends on particle size. ACS Nano 8, 222–233.
Kuempel, E.D., Geraci, C.L., Schulte, P.A., 2012. Risk assessment and risk management of nanomaterials in the workplace: translating research to practice. Ann. Occup. Hyg. 56, 491–505.
Labib, S., Guo, C.H., Williams, A., Yauk, C.L., White, P.A., Halappanavar, S., 2013. Toxicogenomic outcomes predictive of forestomach carcinogenesis following exposure to benzo (a) pyrene: relevance to human cancer risk. Toxicol. Appl. Pharmacol. 273, 269–280.
Labib, S., Williams, A., Yauk, C.L., Nikota, J.K., Wallin, H., Vogel, U., Halappanavar, S., 2016. Nano-risk science: application of toxicogenomics in an adverse outcome pathway framework for risk assessment of multi-walled carbon nanotubes. Particle and Fibre Toxicology 13, 15–31.
Labib, S., Williams, A., Guo, C.H., Leingartner, K., Arlt, V.M., Schmeiser, H.H., Yauk, C.L., White, P.A., Halappanavar, S., 2016a. Comparative transcriptomic analyses to scrutinize the assumption that genotoxic PAHs exert effects via a common mode of action. Arch. Toxicol. 90, 2461–2480.
Lamb, J., Crawford, E.D., Peck, D., Modell, J.W., Blat, I.C., Wrobel, M.J., Lerner, J., Brunet, J.P., Subramanian, A., Ross, K., 2006. N. The Connectivity Map: using gene-expression signatures to connect small molecules, genes, and disease. Science 313,

1929–1935.
Lu, B., Moser, A., Shigenaga, J.K., Grunfeld, C., Feingold, K.R., 2010. The acute phase response stimulates the expression of angiopoietin like protein 4. Biochem. Biophys. Res. Commun. 391, 1737–1741.
Maynard, A.D., Kuempel, E.D., 2005. Airborne nanostructured particles and occupational health. J. Nanopart. Res. 7, 587–614.
Maynard, A.D., Warheit, D.B., Philbert, M.A., 2010. The new toxicology of sophisticated materials: nanotoxicology and beyond. Toxicol. Sci. 120, S109–S129.
Moffat, I., Chepelev, N.L., Labib, S., Bourdon-Lacombe, J., Kuo, B., Buick, J.K., Lemieux, F., Williams, A., Halappanavar, S., Malik, A.I., 2015. Comparison of toxicogenomics and traditional approaches to inform mode of action and points of departure in human health risk assessment of benzo [a] pyrene in drinking water. Crit. Rev. Toxicol. 45, 1–43.
Nikota, J., Williams, A., Yauk, C.L., Wallin, H., Vogel, U., Halappanavar, S., 2015. Meta-analysis of transcriptomic responses as a means to identify pulmonary disease outcomes for engineered nanomaterials. Particle and Fibre Toxicology 13, 25.
Nikota, J., Banville, A., Goodwin, L.R., Wu, D., Williams, A., Yauk, C.L., Wallin, H., Vogel, U., Halappanavar, S., 2017. Stat-6 signaling pathway and not Interleukin-1 mediates multi-walled carbon nanotube-induced lung fibrosis in mice: insights from an adverse outcome pathway framework. Particle and Fibre Toxicology 14, 37–57.
Noel, A., Maghni, K., Cloutier, Y., Dion, C., Wilkinson, K.J., Halle, S., Tardif, R., Truchon, G., 2012. Effects of inhaled nano-TiO2 aerosols showing two distinct agglomeration states on rat lungs. Toxicol. Lett. 214, 109–119.
Oberdoerster, G., Maynard, A., Donaldson, K., Castranova, V., Fitzpatrick, J., Ausman, K., Carter, J., Karn, B., Kreyling, W., Lai, D., 2005. Principles for characterizing the potential human health effects from exposure to nanomaterials: elements of a screening strategy. Particle and Fibre Toxicology 2, 1–35.
Parmigiani, G., Garett, E.S., Irizarry, R.A., Zeger, S.L., 2003. The Analysis of Gene Expression Data, Methods and Software. XIX. Springer-Verlag, New York, pp. 456.
Patlolla, A.K., Hussain, S.M., Schlager, J.J., Patlolla, S., Tchounwou, P.B., 2010. Comparative study of the clastogenicity of functionalized and nonfunctionalized multiwalled carbon nanotubes in bone marrow cells of Swiss-Webster mice. Environ. Toxicol. 25, 608–621.
Pietroiusti, A., Stockmann-Juvala, H., Lucaroni, F., Savolainen, K., 2018. Nanomaterial exposure, toxicity, and impact on human health. Wiley Interdisciplinary Reviews: Nanomedicine and Nanobiotechnology 10, e1513.
Poulsen, S.S., Jacobsen, N.R., Labib, S., Wu, D., Husain, M., Williams, A., Bøgelund, J.P., Andersen, O., Købler, C., Mølhave, K., 2013. Transcriptomic analysis reveals novel mechanistic insight into murine biological responses to multi-walled carbon nanotubes in lungs and cultured lung epithelial cells. PLoS One 8, e80452.
Poulsen, S.S., Saber, A.T., Williams, A., Andersen, O., Koebler, C., Atluri, R., Pozzebon, M.E., Mucelli, S.P., Simion, M., Rickerby, D., 2015. MWCNTs of different physicochemical properties cause similar inflammatory responses, but differences in transcriptional and histological markers of fibrosis in mouse lungs. Toxicol. Appl. Pharmacol. 284, 16–32.
Poulsen, S.S., Jackson, P., Kling, K., Knudsen, K.B., Skaug, V., Kyjovska, Z.O., Thomsen, B.L., Clausen, P.A., Atluri, R., Berthing, T., 2016. Multi-walled carbon nanotube physicochemical properties predict pulmonary inflammation and genotoxicity. Nanotoxicology 10, 1263–1275.
Poulsen, S.S., Knudsen, K.B., Jackson, P., Weydahl, I.E., Saber, A.T., Wallin, H., Vogel, U., 2017. Multi-walled carbon nanotube-physicochemical properties predict the systemic acute phase response following pulmonary exposure in mice. PLoS One 12, e0174167.
Rahman, L., Wu, D., Johnston, M., Williams, A., Halappanavar, S., 2016. Toxicogenomics analysis of mouse lung responses following exposure to titanium dioxide nanomaterials reveal their disease potential at high doses. Mutagenesis 32, 59–76.
Rahman, L., Jacobsen, N.R., Aziz, S.A., Wu, D., Williams, A., Yauk, C.L., White, P., Wallin, H., Vogel, U., Halappanavar, S., 2017. Multi-walled carbon nanotube-induced genotoxic, inflammatory and pro-fibrotic responses in mice: investigating the mechanisms of pulmonary carcinogenesis. Mutation Research/Genetic Toxicology and Environmental Mutagenesis 823, 28–44.
Rittinghausen, S., Hackbarth, A., Creutzenberg, O., Ernst, H., Heinrich, U., Leonhardt, A., Schaudien, D., 2014. The carcinogenic effect of various multi-walled carbon nanotubes (MWCNTs) after intraperitoneal injection in rats. Particle and Fibre Toxicology 11, 59–76.
Ritz, C., Streibig, J.C., 2005. Bioassay analysis using RJ statist. Software 12 (5) (In).
Saber, A.T., Lamson, J.S., Jacobsen, N.R., Ravn-Haren, G., Hougaard, K.S., Nyendi, A.N., Wahlberg, P., Madsen, A.M., Jackson, P., Wallin, H., 2013. Particle-induced pulmonary acute phase response correlates with neutrophil influx linking inhaled particles and cardiovascular risk. PLoS One 8, e69020.
Sager, T.M., Kommineni, C., Castranova, V., 2008. Pulmonary response to intratracheal instillation of ultrafine versus fine titanium dioxide: role of particle surface area. Particle and Fibre Toxicology 5, 17.
Sager, T.M., Wolfarth, M.W., Andrew, M., Hubbs, A., Friend, S., Chen, T.h., Porter, D.W., Wu, N., Yang, F., Hamilton, R.F., 2014. Effect of multi-walled carbon nanotube surface modification on bioactivity in the C57BL/6 mouse model. Nanotoxicology 8, 317–327.
Sargent, L.M., Hubbs, A.F., Young, S.H., Kashon, M.L., Dinu, C.Z., Salisbury, J.L., Benkovic, S.A., Lowry, D.T., Murray, A.R., Kisin, E.R., 2012. Single-walled carbon nanotube-induced mitotic disruption. Mutation Research/Genetic Toxicology and Environmental Mutagenesis 745, 28–37.
Sargent, L.M., Porter, D.W., Staska, L.M., Hubbs, A.F., Lowry, D.T., Battelli, L., Siegrist, K.J., Kashon, M.L., Mercer, R.R., Bauer, A.K., 2014. Promotion of lung adenocarcinoma following inhalation exposure to multi-walled carbon nanotubes. Particle and Fibre Toxicology 11, 3–20.
Sauer, U.G., Deferme, L., Gribaldo, L., Hackermüller, J., Tralau, T., van Ravenzwaay, B., Yauk, C., Poole, A., Tong, W., Gant, T.W., 2017. The challenge of the application of 'omics technologies in chemicals risk assessment: background and outlook. Regul. Toxicol. Pharmacol. 91, S14–S26.
Sayes, C.M., Reed, K.L., Warheit, D.B., 2007. Assessing toxicity of fine and nanoparticles: comparing in vitro measurements to in vivo pulmonary toxicity profiles. Toxicol. Sci. 97, 163–180.
Schmid, O., Cassee, F.R., 2017. On the pivotal role of dose for particle toxicology and risk assessment: exposure is a poor surrogate for delivered dose. Particle and Fibre Toxicology 14, 1–5.
Schmid, O., Stoeger, T., 2016. Surface area is the biologically most effective dose metric for acute nanoparticle toxicity in the lung. J. Aerosol Sci. 99, 133–143.
Sweeney, S., Berhanu, D., Ruenraroengsak, P., Thorley, A.J., Valsami-Jones, E., Tetley, T.D., 2015. Nano-titanium dioxide bioreactivity with human alveolar type-I-like epithelial cells: investigating crystalline phase as a critical determinant. Nanotoxicology 9, 482–492.
Takagi, A., Hirose, A., Futakuchi, M., Tsuda, H., Kanno, J., 2012. Dose-dependent mesothelioma induction by intraperitoneal administration of multi-wall carbon nanotubes in p53 heterozygous mice. Cancer Sci. 103, 1440–1444.
Team, R. C. 2014. R: A Language and Environment for Statistical Computing. R Foundation for Statistical Computing, Vienna, Austria. 2013. (In).
Thomas, R.S., Allen, B.C., Nong, A., Yang, L., Bermudez, E., Clewell III, H.J., Andersen, M.E., 2007. A method to integrate benchmark dose estimates with genomic data to assess the functional effects of chemical exposure. Toxicol. Sci. 98, 240–248.
Thomas, R.S., Clewell III, H.J., Allen, B.C., Wesselkamper, S.C., Wang, N.C., Lambert, J.C., Hess-Wilson, J.K., Zhao, Q.J., Andersen, M.E., 2010. Application of transcriptional benchmark dose values in quantitative cancer and noncancer risk assessment. Toxicol. Sci. 120, 194–205.
Thomas, R.S., Clewell, H.J., Allen, B.C., Yang, L., Healy, E., Andersen, M.E., 2012. Integrating pathway-based transcriptomic data into quantitative chemical risk assessment: a five chemical case study. Mutation Research/Genetic Toxicology and Environmental Mutagenesis 746, 135–143.
Ursini, C.L., Maiello, R., Ciervo, A., Fresegna, A.M., Buresti, G., Superti, F., Marchetti, M., Iavicoli, S., Cavallo, D., 2016. Evaluation of uptake, cytotoxicity and inflammatory effects in respiratory cells exposed to pristine and -OH and -COOH functionalized multi-wall carbon nanotubes. J. Appl. Toxicol. 36, 394–403.
Warheit, D. B.(2018) Hazard and risk assessment strategies for nanoparticle exposures: how far have we come in the past 10 years? F1000Research, 7, 376–389.
Warheit, D.B., Webb, T.R., Reed, K.L., Frerichs, S., Sayes, C.M., 2007. Pulmonary toxicity study in rats with three forms of ultrafine-TiO2 particles: differential responses related to surface properties. Toxicology 230, 90–104.
Wu, H., Kerr, M.K., Cui, X., Churchill, G.A., 2003. MAANOVA: a software package for the analysis of spotted cDNA microarray experiments. In: The Analysis of Gene Expression Data. Springer, pp. 313–341.
Yang, Y.H., Dudoit, S., Luu, P., Lin, D.M., Peng, V., Ngai, J., Speed, T.P., 2002. Normalization for cDNA microarray data: a robust composite method addressing single and multiple slide systematic variation. Nucleic Acids Res. 30, e15.
Yann, G., Dana, L., Guyton, K.Z., Secretan, B.a.L., El Ghissassi, F., Véronique, B., Tallaa, L.B., Neela, G., Chiara, S., Heidi, M., 2014. Carcinogenicity of fluoro-edenite, silicon carbide fibres and whiskers, and carbon nanotubes. Lancet Oncol. 15, 1427–1428.

Update

NanoImpact

Volume 21, Issue , January 2021, Page

DOI: https://doi.org/10.1016/j.impact.2020.100284

NanoImpact 21 (2021) 100284

Contents lists available at ScienceDirect

NanoImpact

journal homepage: www.elsevier.com/locate/nanoimpact

Erratum regarding missing Declaration of Competing Interest statements in previously published articles

The **Declaration of Competing Interest** statements were not included in the published version of the following articles that appeared in previous issues of NanoImpact. The appropriate Declaration \Competing Interest statements, provided by authors, are included below.

1. "An electrochemical method to rapidly assess the environmental risk of silver release from nanowire transparent conductive films" (NanoImpact, 2020; 18C: 100217) doi:https://doi.org/10.1016/j.impact.2020.100217 Declaration of competing interest: The authors were contacted after publication to request a Declaration of Interest statement.
2. "The method of depositing CeO2 nanoparticles onto a DPPC monolayer affects surface tension behaviour" (NanoImpact, 2019; 16C: 100186) doi:https://doi.org/10.1016/j.impact.2019.100186 Declaration of competing interest: The authors declare that they have no known competing financial interests or personal relationships that could have appeared to influence the work reported in this paper.
3. "Key challenges for evaluation of the safety of engineered nanomaterials" (NanoImpact, 2020; 18C: 100219) doi:https://doi.org/10.1016/j.impact.2020.100219 Declaration of competing interest: The authors declare that they have no known competing financial interests or personal relationships that could have appeared to influence the work reported in this paper.
4. "Scientific rationale for the development of an OECD test guideline on engineered nanomaterial stability" (NanoImpact, 2018; 11C: 42–50) doi:https://doi.org/10.1016/j.impact.2018.01.003 Declaration of competing interest: The authors were contacted after publication to request a Declaration of Interest statement.
5. "Chemical and physical transformations of silver nanomaterial containing textiles after modeled human exposure" (NanoImpact, 2019; 14C: 100160) doi:https://doi.org/10.1016/j.impact.2019.100160 Declaration of competing interest: The authors declare that they have no known competing financial interests or personal relationships that could have appeared to influence the work reported in this paper.
6. "Quality in nanosafety —Towards reliable nanomaterial safety assessment" (NanoImpact, 2018; 11C: 67–68) doi:https://doi.org/10.1016/j.impact.2018.02.005 Declaration of competing interest: The authors were contacted after publication to request a Declaration of Interest statement.
7. "Directions in QPPR development to complement the predictive models used in risk assessment of nanomaterials" (NanoImpact, 2018; 11C: 58–66) doi:https://doi.org/10.1016/j.impact.2018.02.003 Declaration of competing interest: The authors declare that they have no known competing financial interests or personal relationships that could have appeared to influence the work reported in this paper.
8. "Co-exposure of imidacloprid and nanoparticle Ag or CeO2 to *Cucurbita pepo* (zucchini): Contaminant bioaccumulation and translocation" (NanoImpact, 2018; 11C: 136–145) doi:https://doi.org/10.1016/j.impact.2018.07.001 Declaration of competing interest: The authors declare that they have no known competing financial interests or personal relationships that could have appeared to influence the work reported in this paper.
9. "Modelling engineered nanomaterials in wet-weather discharges" (NanoImpact, 2019; 16C: 100188) doi:https://doi.org/10.1016/j.impact.2019.100188 Declaration of competing interest: The authors declare that they have no known competing financial interests or personal relationships that could have appeared to influence the work reported in this paper.
10. "Long-term outdoor lysimeter study with cerium dioxide nanomaterial"(NanoImpact, 2019; 14C: 100170) doi:https://doi.org/10.1016/j.impact.2019.100170 Declaration of competing interest: The authors were contacted after publication to request a Declaration of Interest statement.
11. "Determination of the delivered dose of nanoparticles in the trachea-bronchial and alveolar regions of the lung" (NanoImpact, 2019; 14C: 100162) doi:https://doi.org/10.1016/j.impact.2019.100162 Declaration of competing interest: The authors declare that they have no known competing financial interests or personal relationships that could have appeared to influence the work reported in this paper.

DOIs of original article: https://doi.org/10.1016/j.impact.2019.100163, https://doi.org/10.1016/j.impact.2020.100217, https://doi.org/10.1016/j.impact.2019.100188, https://doi.org/10.1016/j.impact.2019.100158, https://doi.org/10.1016/j.impact.2020.100219, https://doi.org/10.1016/j.impact.2019.100162, https://doi.org/10.1016/j.impact.2018.01.003, https://doi.org/10.1016/j.impact.2019.100160, https://doi.org/10.1016/j.impact.2018.02.005, https://doi.org/10.1016/j.impact.2019.100193, https://doi.org/10.1016/j.impact.2019.100186, https://doi.org/10.1016/j.impact.2018.02.003, https://doi.org/10.1016/j.impact.2019.100170, https://doi.org/10.1016/j.impact.2018.07.001, https://doi.org/10.1016/j.impact.2019.100151.

https://doi.org/10.1016/j.impact.2020.100284

Available online 15 December 2020

12. “Comparative multi-generation study on long-term effects of pristine and wastewater-borne silver and titanium dioxide nanoparticles on key lifecycle parameters in *Daphnia magna*” (NanoImpact, 2019; 14C: 100163) doi:https://doi.org/10.1016/j.impact.2019.100163 Declaration of competing interest: The authors were contacted after publication to request a Declaration of Interest statement.
13. “UV-induced over time transformation of AgNPs in commercial wound dressings and adverse biological effects on *Caenorhabditis elegans*” (NanoImpact, 2019; 17C: 100193) doi:https://doi.org/10.1016/j.impact.2019.100193 Declaration of competing interest: The authors were contacted after publication to request a Declaration of Interest statement.
14. “Ranking of nanomaterial potency to induce pathway perturbations associated with lung responses” (NanoImpact, 2019; 14C: 100158) doi:https://doi.org/10.1016/j.impact.2019.100158 Declaration of competing interest: The authors declare that they have no known competing financial interests or personal relationships that could have appeared to influence the work reported in this paper.
15. “Surface coating determines the response of soybean plants to cadmium sulfide quantum dots” (NanoImpact, 2019; 14C: 100151) doi:https://doi.org/10.1016/j.impact.2019.100151 Declaration of competing interest: The authors declare that they have no known competing financial interests or personal relationships that could have appeared to influence the work reported in this paper.